NASA TN D-17

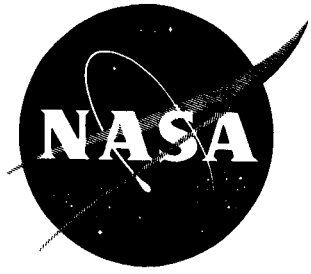

TECHNICAL NOTE
D-17

WIND-TUNNEL INVESTIGATION OF EFFECT OF RATIO OF WING CHORD TO PROPELLER DIAMETER WITH ADDITION OF SLATS ON THE AERODYNAMIC CHARACTERISTICS OF TILT-WING VTOL CONFIGURATIONS IN THE TRANSITION SPEED RANGE

By Robert T. Taylor

Langley Research Center
Langley Field, Va.

NATIONAL AERONAUTICS AND SPACE ADMINISTRATION
WASHINGTON
September 1959

NATIONAL AERONAUTICS AND SPACE ADMINISTRATION

TECHNICAL NOTE D-17

WIND-TUNNEL INVESTIGATION OF EFFECT OF RATIO OF WING CHORD TO PROPELLER DIAMETER WITH ADDITION OF SLATS ON THE AERODYNAMIC CHARACTERISTICS OF TILT-WING VTOL CONFIGURATIONS IN THE TRANSITION SPEED RANGE

By Robert T. Taylor

SUMMARY

An investigation has been made in the Langley 300-MPH 7- by 10-foot tunnel to determine the effect of changes in wing chord and the effect of addition of 0.15c leading-edge slats on the longitudinal aerodynamic characteristics of a small wing-propeller combination simulating a twin-engine, tilt-wing, vertical-take-off-and-landing aircraft.

Increases in wing chord serve to reduce the severity of the stall in the transition speed range. Extending a 0.15c leading-edge slat also decreases the severity of the stall but in some cases gives sizable nose-up pitching moments.

INTRODUCTION

One method of attaining vertical take-off and landing with a more or less conventional cruising configuration is the so-called "tilt-wing" arrangement. With this arrangement the wing-engine-propeller combination tilts 90° so that the propeller thrust opposes the weight of the machine in the hovering condition. In cruising flight the combination is arranged conventionally. Previous investigations (refs. 1 and 2) have shown that the stall in the region of transition flight between hovering and the speed for minimum power is a major factor affecting the power requirements in the transition speed range. It is also likely that control difficulties may be encountered with the wing partially stalled.

The local angles of attack that the wing experiences in transition arise from the vector addition of the free-stream and propeller slipstream velocities. The propeller slipstream is seen to be a strong factor in decreasing the local angles of attack of the wing and therefore in minimizing the tendency of the wing to stall. However, if the slipstream velocity is too low (because of low disk loading, for instance) stall may

be encountered even in the presence of the slipstream. This sort of qualitative reasoning indicates that stalling tendencies of tilt-wing configurations should be decreased by increasing either the propeller disk loading or the wing area.

The present investigation was undertaken to obtain quantitative information on the effect of the ratio of wing size to propeller size on tilt-wing stalling characteristics. In order to simplify the investigation the tests were made by varying the wing chord behind a propeller of constant disk loading and size.

Reference 3 indicates that a leading-edge slat could be effective in delaying the stall of configurations equipped with large-chord flaps in the transition speed range. The effectiveness of leading-edge slats in delaying the stall of tilt-wing configurations is also included in the present investigation.

SYMBOLS

Figure 1 presents the directions of positive forces, moments, and angles.

b propeller blade chord, ft

$C_{D,o}$ profile drag coefficient

$C_{L,s}$ lift coefficient, $\dfrac{\text{Lift}}{q_s \frac{S}{2}}$

$C_{m,s}$ pitching-moment coefficient, $\dfrac{\text{Pitching moment about } c/4}{q_s \frac{S}{2} c}$

C_P power coefficient, $\dfrac{2\pi Qn}{\rho n^3 D^5}$

C_T thrust coefficient, $\dfrac{T}{\rho n^2 D^4}$

$C_{T,s}$ thrust coefficient, $\dfrac{T}{q_s \frac{\pi}{4} D^2}$

$C_{X,s}$ longitudinal-force coefficient, $\dfrac{\text{Longitudinal force}}{q_s \frac{S}{2}}$

c	wing chord, ft
D	propeller diameter, ft
h	propeller blade thickness, ft
J	advance ratio, V/nD
n	propeller rotational speed, rps
P	propeller shaft power, $\frac{2\pi Qn}{550}$, hp
Q	propeller shaft torque, ft-lb
q	free-stream dynamic pressure, $\frac{1}{2}\rho V^2$, lb/sq ft
q_s	slipstream dynamic pressure, $q + \frac{T}{\frac{\pi D^2}{4}}$, lb/sq ft
R	propeller tip radius, ft
r	radius to propeller blade element, ft
S	total wing area, sq ft
T	propeller shaft thrust, lb
V	free-stream velocity, ft/sec, unless otherwise indicated
W	airplane weight, lb
α	angle of attack, deg
$\beta_{.75}$	propeller blade angle at 0.75R, deg
η	propeller efficiency, $\frac{TV}{2\pi nQ}$
η'	propeller effectiveness, $\eta \frac{\cos\alpha + \sqrt{\cos^2\alpha + \frac{8C_T}{\pi J^2}}}{2}$

η_{st} static thrust efficiency, $\frac{T^{3/2}}{1100P\sqrt{\frac{\rho}{2}\frac{\pi D^2}{4}}}$

ρ mass density of air, slugs/cu ft

MODELS AND APPARATUS

The wing span, propeller diameter, and propeller thrust were held constant to assess the effect of changes in wing chord. Changes in wing chord brought accompanying changes in aspect ratio and wing area. The geometric characteristics of the three models used are given in the following table:

Model	c/D	Area, sq ft	Chord, ft	Aspect ratio
A	0.33	1.667	0.667	7.50
B	.50	2.500	1.000	5.00
C	.75	3.750	1.500	3.33

The models each had an NACA 0015 airfoil section with a revolved tip. Sketches of the models and ordinates of the slat are given in figure 2, and a photograph of model B mounted in the Langley 300-MPH 7- by 10-foot tunnel is shown in figure 3. The propeller blade-form curves are given in figure 4. The propeller used in these tests is a three-bladed version of that used in the investigation of reference 4.

Measurements were made of the longitudinal force and moment characteristics of the wing-nacelle-propeller combination through the angle-of-attack and speed range, by means of a three-component strain-gage balance to which the root of the wing was attached. Separate measurements of propeller thrust and torque were made by means of strain-gage beams which held a variable-frequency electric motor securely to the inside of the nacelle. This system is described in detail in reference 1. The rotational speed of the propeller was determined by feeding the output of a small shaft-connected alternator into a stroboscopic instrument.

TESTS

The tests were made in the Langley 300-MPH 7- by 10-foot tunnel at various free-stream dynamic pressures and propeller thrusts so as to maintain a constant slipstream dynamic pressure of 8 pounds per square foot. The experimental propeller efficiencies (fig. 5) were determined with the propeller mounted on wing B for two blade angles at an angle of attack of 0°. During the tests the propeller thrust was held constant through an angle-of-attack range by allowing the speed of the motor to vary.

The range of the variables investigated was: $C_{T,s}$, 0 to 0.98; α, -10° to 120°; and c/D, 0.33 to 0.75. The tests were run at Reynolds numbers of 352,000 for model A, 530,000 for model B, and 795,000 for model C, based on wing chord and average slipstream velocity.

CORRECTIONS

Corrections to the velocity due to the propeller operation were made by the method of reference 1.

Estimates of the errors due to stream boundaries were made and found to be negligible. The errors due to blockage were estimated and were found to be negligible except at the combined conditions of high angle of attack and high velocity. Inasmuch as these conditions are unrealistic, blocking corrections have not been applied.

RESULTS AND DISCUSSION

Wind-Tunnel Results

The results of the investigation are presented in the following figures:

The data for the propeller at the blade angles used are presented in figure 6 with the propeller mounted ahead of wing C, to show the change of the coefficients with angle of attack. The propeller effectiveness η' is not shown for $C_{T,s} = 1.0$ because the effectiveness η' reduces to the static thrust efficiency (figure of merit) η_{st} as the thrust coefficient attains a value of unity (hovering).

The basic data for the three configurations tested are presented in figures 7 to 9. The lift coefficient available for climbing, level, and descending flight may be obtained directly from the polars of lift coefficient and longitudinal-force coefficient presented in these figures. Zero longitudinal-force coefficient indicates a thrust-drag balance and therefore a steady level flight condition. Negative values of $C_{X,s}$ indicate an excess of drag and therefore decelerating or descending flight, whereas positive values of $C_{X,s}$ indicate excess thrust and accelerating or climbing flight.

In general, with power on, maximum lift occurs in the region of level flight $(C_{X,s} = 0)$ and the lift decreases progressively in the descending flight region $(-C_{X,s})$, indicating that the wing is stalled.

Tuft studies such as those shown in figure 10 indicate that the stall is gradual and progressive, with appreciable separation present in the level-flight region and some separation apparent well down on the climbing-flight leg of the curve. The photographs show the progression of the stall through the wing-attitude range near $C_{X,s} = 0$ at thrust coefficients of 0.88 and 0.58. The corresponding data points are shown shaded in figure 8(b) and 8(c). Propeller rotational direction was selected to counter the tip vortex of the wing. As a result of the twist in the propeller slipstream, tufts outboard of the engine nacelle show steady air flow to much higher angles of attack than tufts inboard of the nacelle. The effect of the leading-edge slat on stall alleviation may also be seen in the photographs of figure 10.

The addition of a slat to each of the wings increased the maximum lift and suppressed the separation, but was not adequate to eliminate completely the separation in the level-flight region for any of the wings tested. The slat position was determined from preliminary tests of various positions and deflections at a thrust coefficient $C_{T,s}$ of about 0.90. The data indicate, however, that the stall is worse at a somewhat lower thrust coefficient, and possibly a better slat configuration could be found. Both the present tests and those of reference 2 indicate that a slat with a large chord, located ahead of and well above the wing, is needed for stall control in the transition flight regime. This slat position suggests that the additional area supplied by the slat is also a prime factor in the increase of lift.

Additional data on a tilt-wing airplane model are presented in reference 5. The data of reference 5 show less severe stall than the data of the present paper; however, it is felt that the cutout in the center section of the wing of the model used in reference 5 decreases the effective aspect ratio and thereby enables the wing to reach higher angles of attack before stalling.

Calculations for Assumed Airplane

The effects of changes in wing chord and the effect of the slat is best illustrated by curves of the power required for an assumed airplane. The curves presented in figures 11 and 12 were calculated by the method of reference 1 from the data of the present paper. The airplane assumed had the characteristics listed in table I.

Effect of chord-diameter ratio.- Figure 11 presents graphically the effects of changes in the ratio of wing chord to propeller diameter on the horsepower required to maintain steady level flight at various speeds. Increases in c/D lower the stalling speed, because of decreases in W/S, and decrease the severity of the stall in the transition speed range. This decrease in the severity of stall results in less required power at a given speed. From figure 11 it would seem that at values of c/D somewhere below 0.33 the cost in power due to stall could exceed the power required for hovering or possibly even the power installed in the airplane. The latter situation would preclude transition to steady level flight.

Effect of slat.- Figure 12 shows the effect on power required of extending the 0.15c slat on the three wings in question. The slat reduces the power required in the transition speed range for all the wings, but the effect decreases with increasing c/D (decreasing aspect ratio).

Extension of the slat would be expected to cause a change in the maximum untrimmed pitching moment for a given wing. Figure 13 shows that with wing A (c/D - 0.33) a relatively small elevator deflection will be required to control the slat-generated pitching moment, whereas with wing C (c/D - 0.75) the control requirements increase almost 50 percent when the slat is extended. The foregoing discussion would indicate that little reason exists for using slats (at least in the configuration tested) when the ratio of wing chord to propeller diameter approaches 0.75. Possibly a more realistic approach might lie in the use of trailing-edge flaps (as indicated in ref. 1) to control the stall and to alleviate to some extent the longitudinal-control difficulties during transition.

The effectiveness of a horizontal tail in trimming these moments cannot be determined from the tuft-grid photographs presented in figure 14;

however they do give an indication of the character of the flow field in which the horizontal tail would have to operate. The tuft grid was located 3 wing-chord lengths behind the model.

CONCLUDING REMARKS

An investigation has been made in the Langley 300-MPH 7- by 10-foot tunnel to determine the effect of changes in wing chord and the effect of the addition of a 0.15c leading-edge slat on the longitudinal aerodynamic characteristics of a small-scale wing-propeller combination simulating a twin-engine, tilt-wing, vertical-take-off-and-landing aircraft. In the investigation it has been found that increases in wing chord serve to reduce the severity of the stall in the transition speed range. Extending a 0.15c leading-edge slat also decreases the severity of the stall, but in some cases gives sizable nose-up increments in pitching moment.

Langley Research Center,
National Aeronautics and Space Administration,
Langley Field, Va., April 8, 1959.

REFERENCES

1. Kuhn, Richard E., and Draper, John W.: Investigation of the Aerodynamic Characteristics of a Model Wing-Propeller Combination and of the Wing and Propeller Separately at Angles of Attack up to 90°. NACA Rep. 1263, 1956. (Supersedes NACA TN 3304 by Draper and Kuhn.)

2. Kuhn, Richard E.: Take-Off and Landing Distance and Power Requirements of Propeller-Driven STOL Airplanes. Preprint No. 690, S.M.F. Pub. Fund Preprint, Inst. Aero. Sci., Inc., Jan. 1957.

3. Kuhn, Richard E., and Hayes, William C., Jr.: Wind-Tunnel Investigation of Effect of Propeller Slipstreams on Aerodynamic Characteristics of a Wing Equipped With a 50-Percent-Chord Sliding Flap and a 30-Percent-Chord Slotted Flap. NACA TN 3918, 1957.

4. McLemore, H. Clyde, and Cannon, Michael D.: Aerodynamic Investigation of a Four-Blade Propeller Operating Through an Angle-of-Attack Range From 0° to 180°. NACA TN 3228, 1954.

5. Newsom, William A., Jr., and Tosti, Louis P.: Force-Test Investigation of the Stability and Control Characteristics of a 1/4-Scale Model of a Tilt-Wing Vertical-Take-Off-and-Landing Aircraft. NASA MEMO 11-3-58L, 1959.

TABLE I

CHARACTERISTICS OF ASSUMED AIRPLANE

Gross weight, lb	2,500
Span, ft	25
Span loading, lb/ft	100
Span efficiency factor	0.80
Taper ratio	1.0
Sweep, deg	0
Propeller diameter, ft	10

	Wing A	Wing B	Wing C
Area, sq ft	83.3	125.0	187.5
Wing loading, lb/sq ft	30	20	13.3
$C_{D,o}S$, sq ft	2.7	3.11	3.75
Ratio of wing chord to propeller diameter	0.33	0.50	0.75

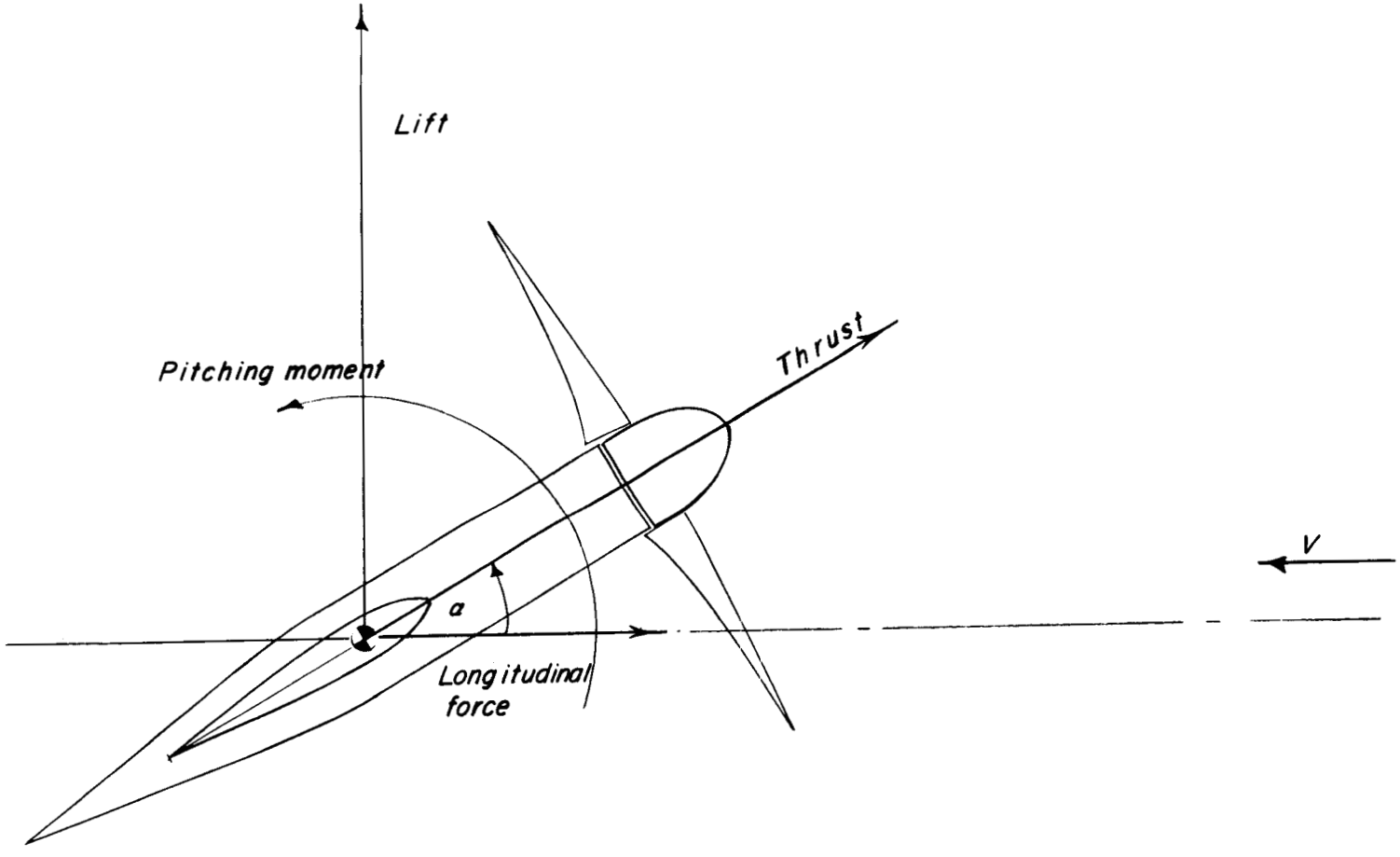

Figure 1.- The positive sense of forces, moments, and angles.

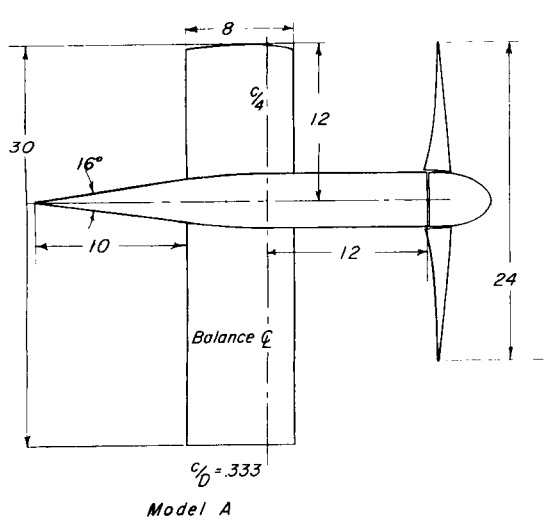

Model A

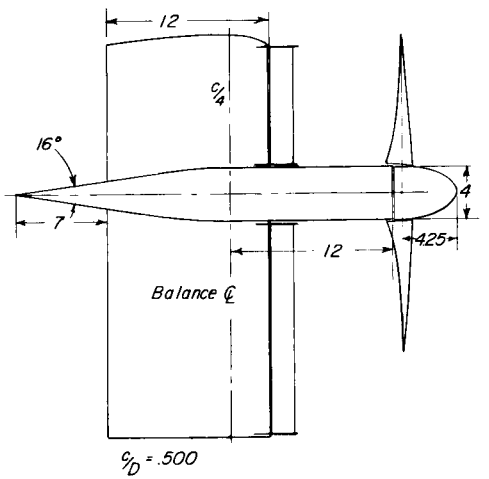

(Drawn with slat extended)

Model B

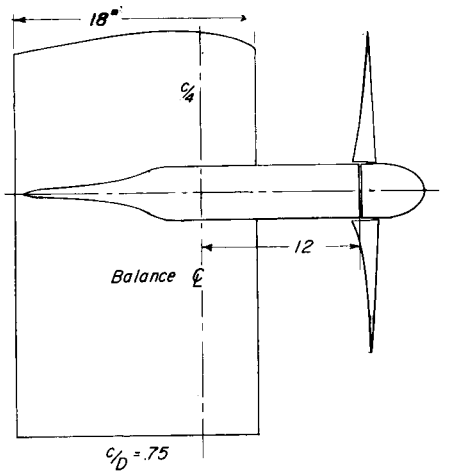

Model C

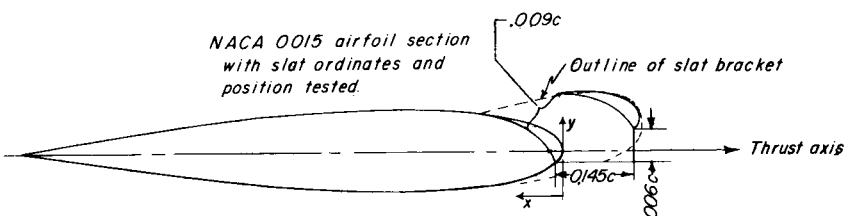

Slat lower-surface ordinates as fractions of the chord
(Given from wing chord plane)

x	y
0	0
.02	-.0295
.025	-.0066
.04	.0200
.075	.0388
.10	.0510
.15	.0661

Figure 2.- Wing and slat geometry of the models. All nacelles are identical; 16° tail cone fairs smoothly into motor housing. All dimensions are in inches unless otherwise noted.

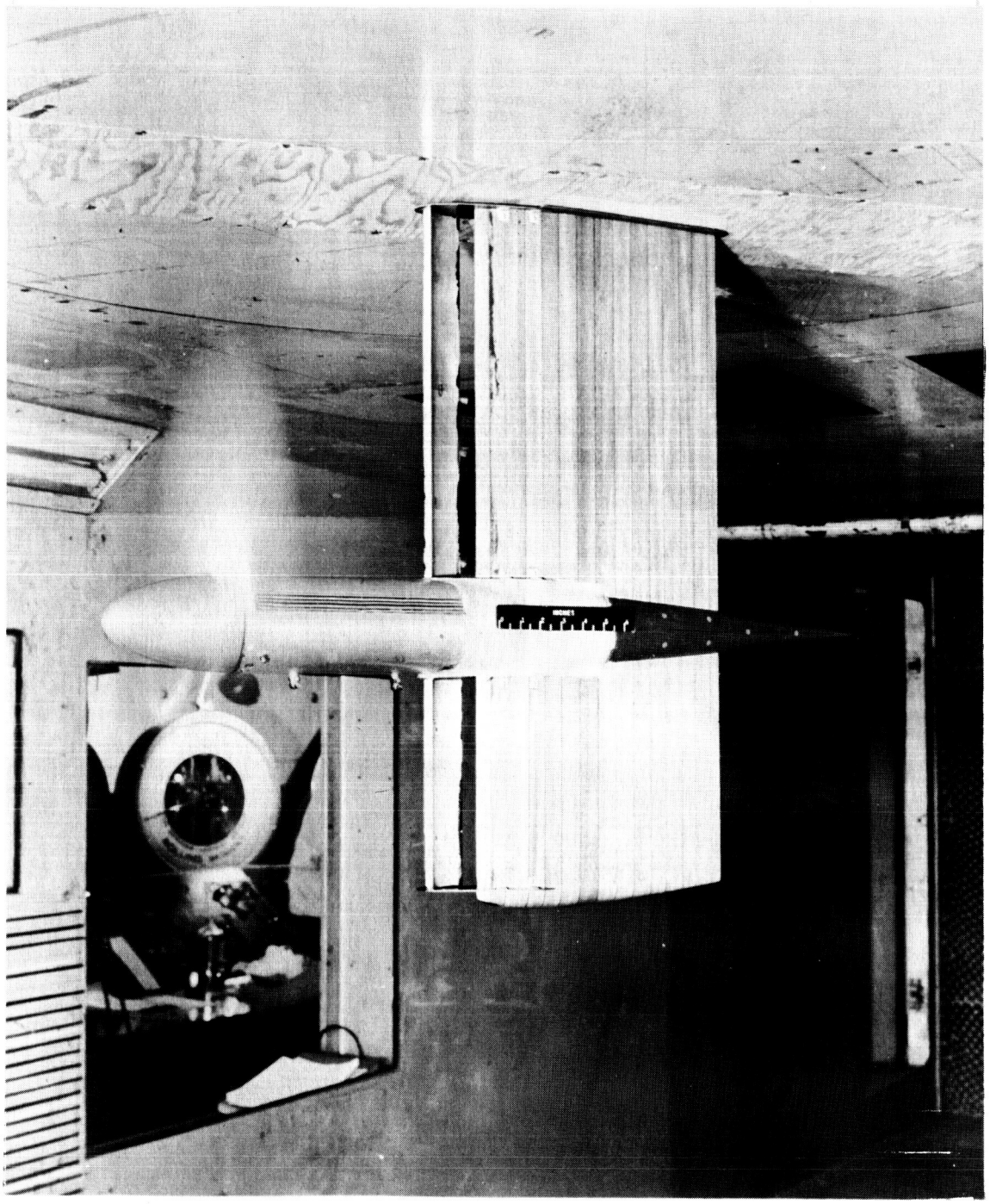

L-95095

Figure 3.- Photograph of model B in 300-MPH 7- by 10-foot tunnel.

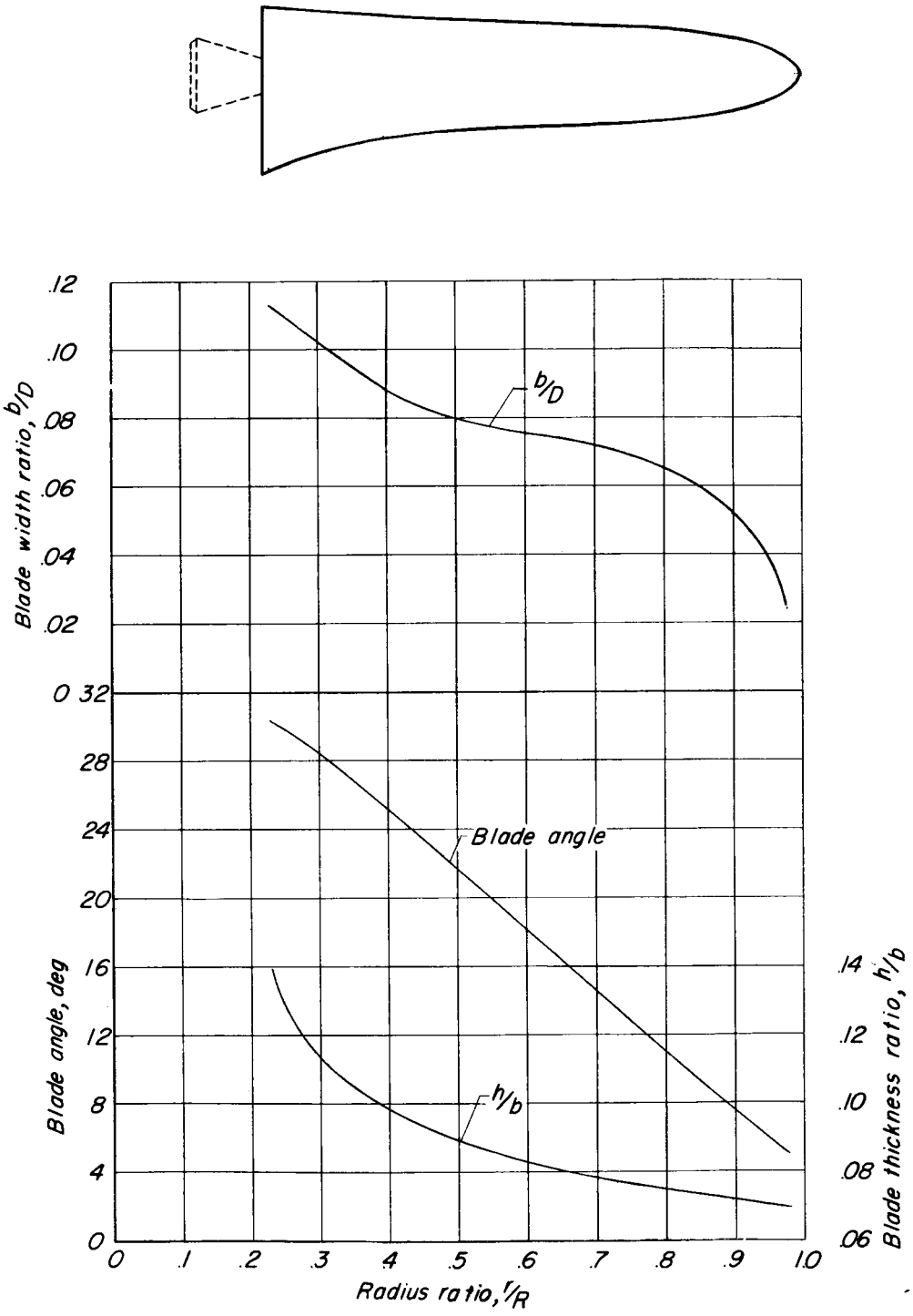

Figure 4.- Propeller blade-form curves (16-series section).

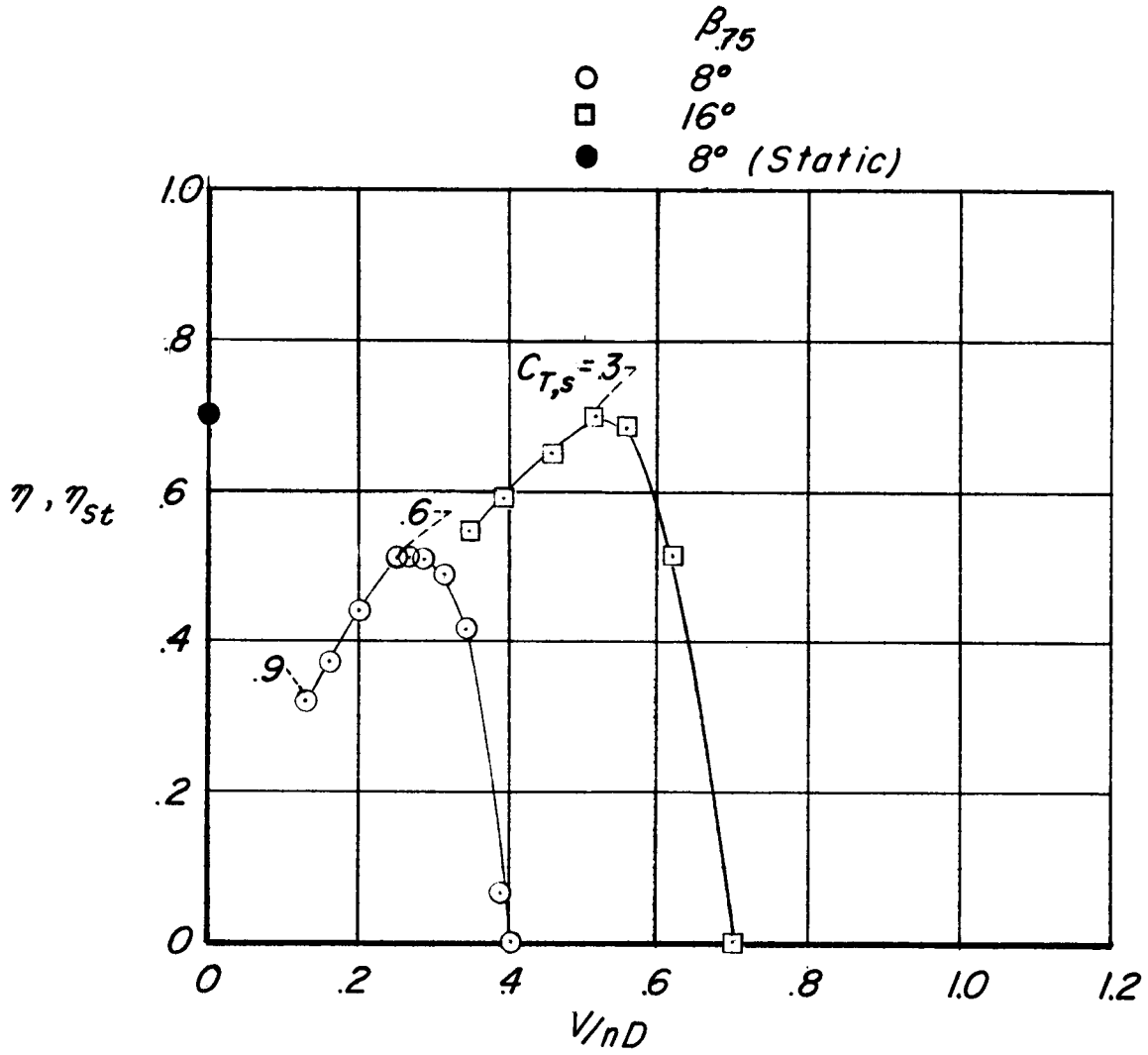

Figure 5.- Variation of propeller efficiency with advance ratio for the blade angles used. $\alpha = 0^{\circ}$; c/D = 0.50.

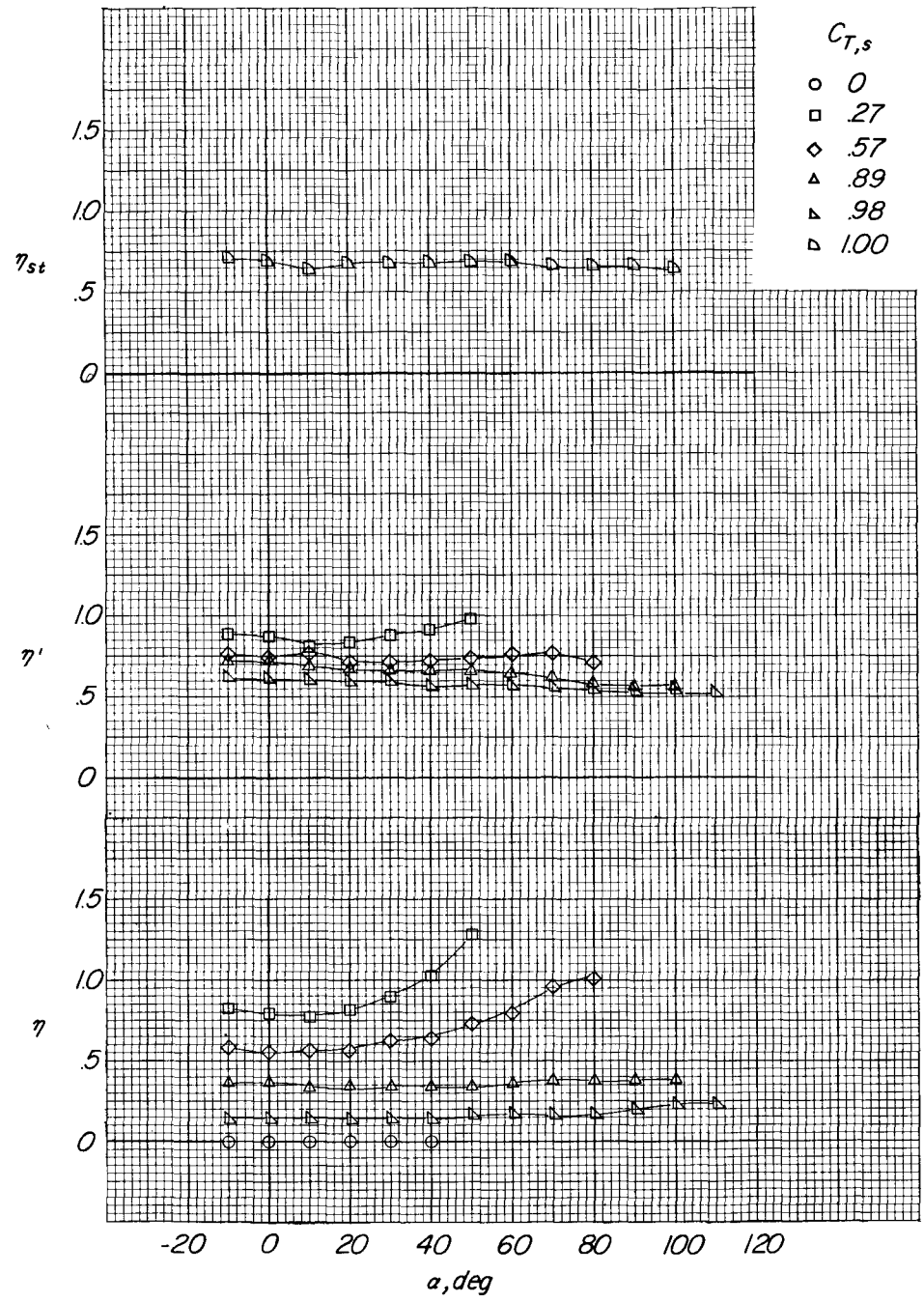

(a) Propeller efficiencies.

Figure 6.- Variation of the propeller characteristics with angle of attack through the range of $C_{T,s}$. c/D = 0.75.

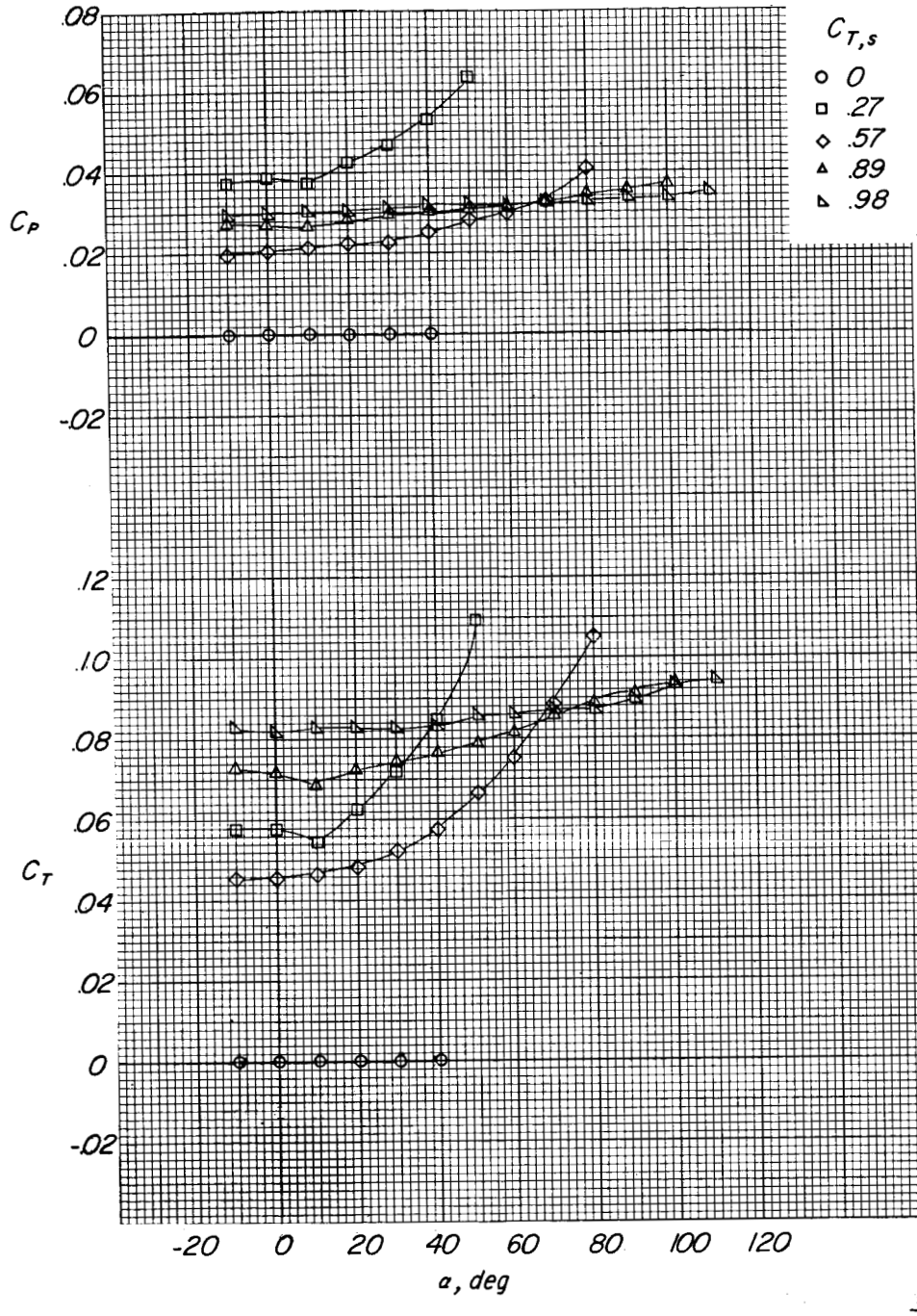

(b) Propeller thrust and power coefficients.

Figure 6.- Continued.

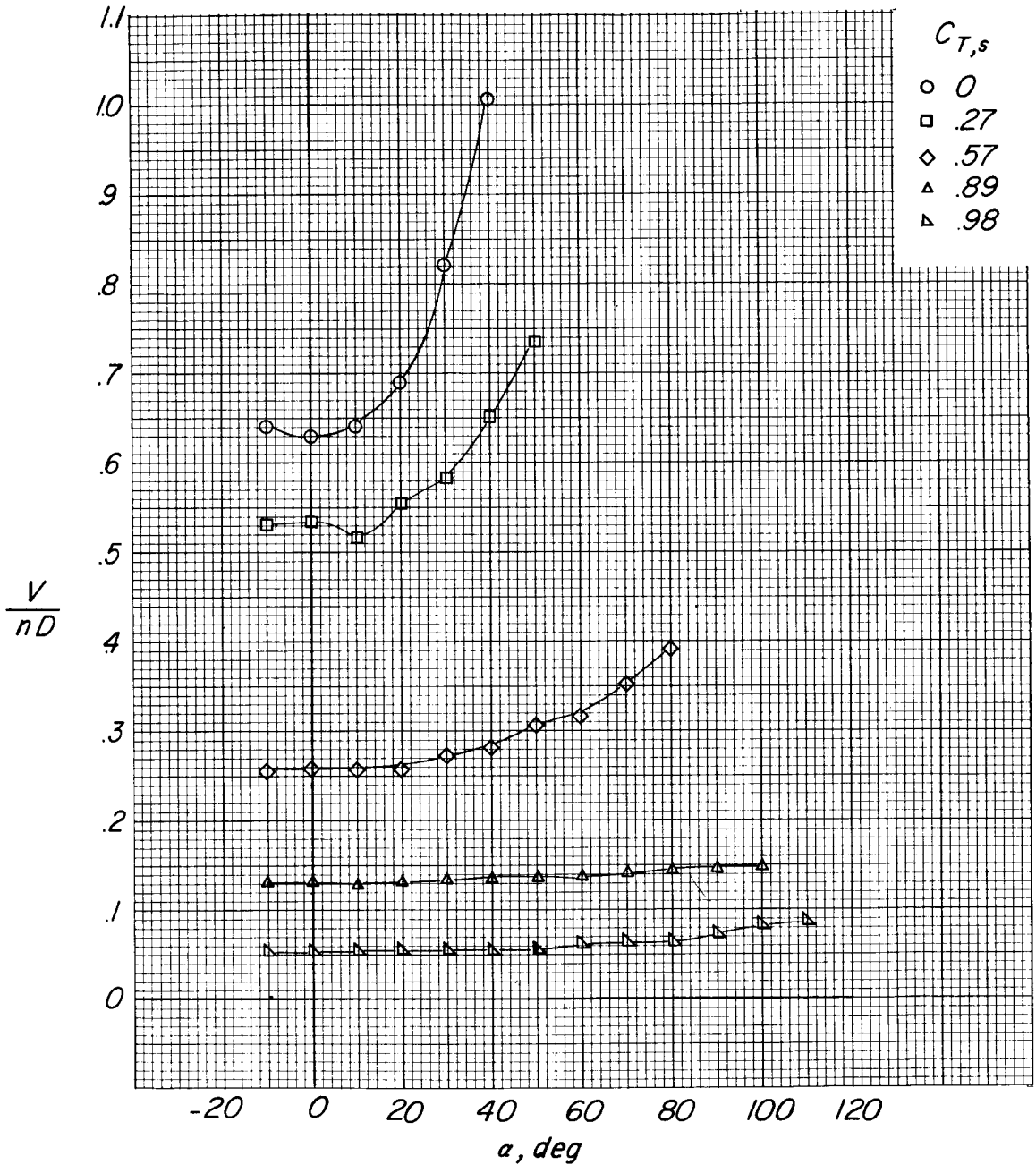

(c) Propeller advance ratio.

Figure 6.- Concluded.

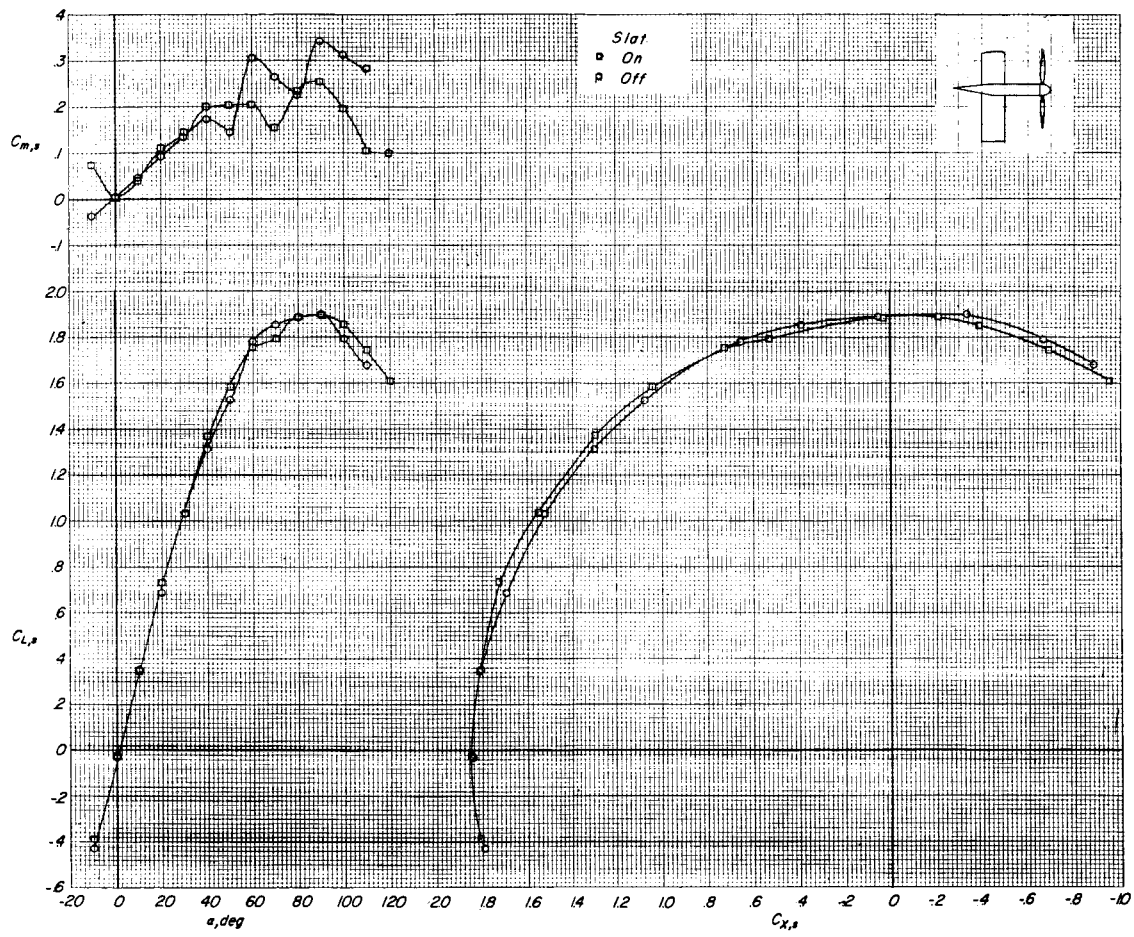

(a) $C_{T,s} = 0.98$.

Figure 7.- Longitudinal aerodynamic characteristics of model A (c/D = 0.33).

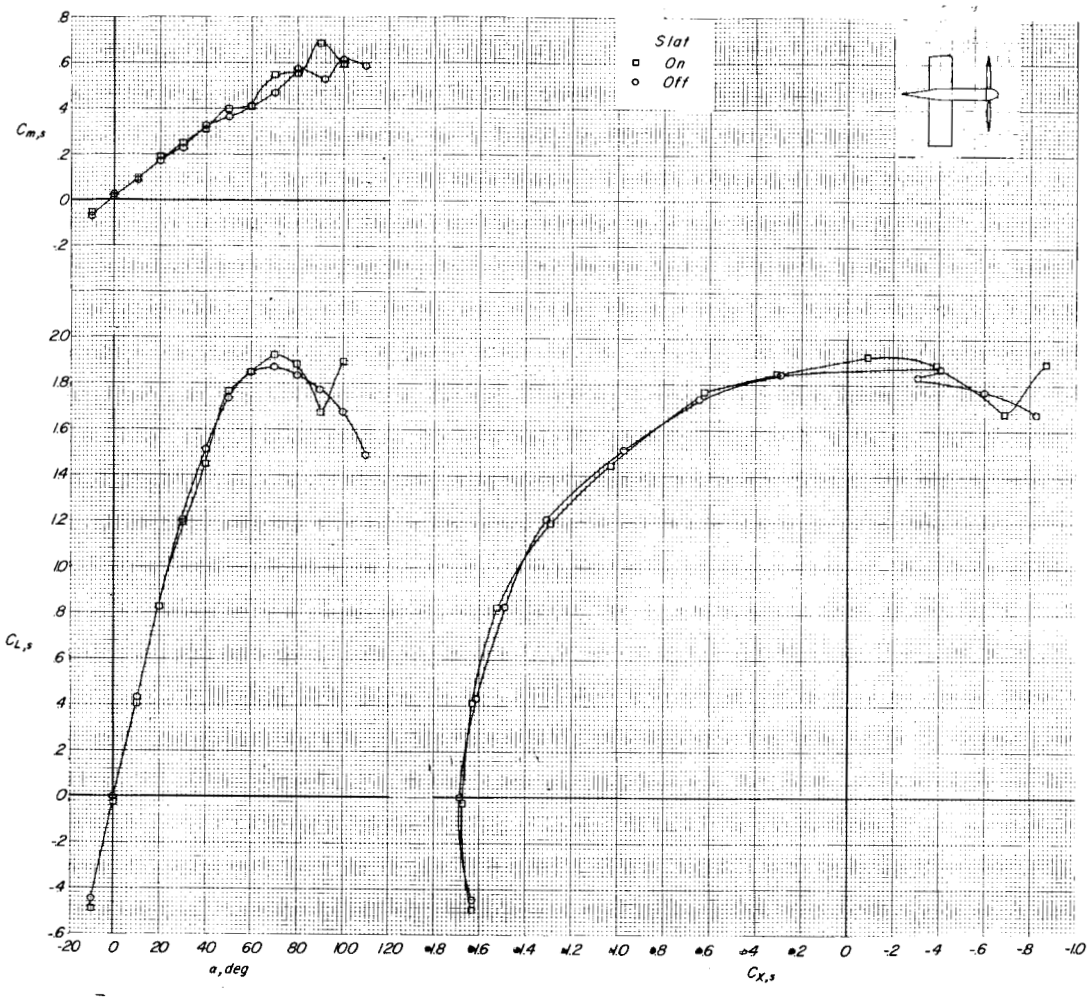

(b) $C_{T,s} = 0.89$.

Figure 7.- Continued.

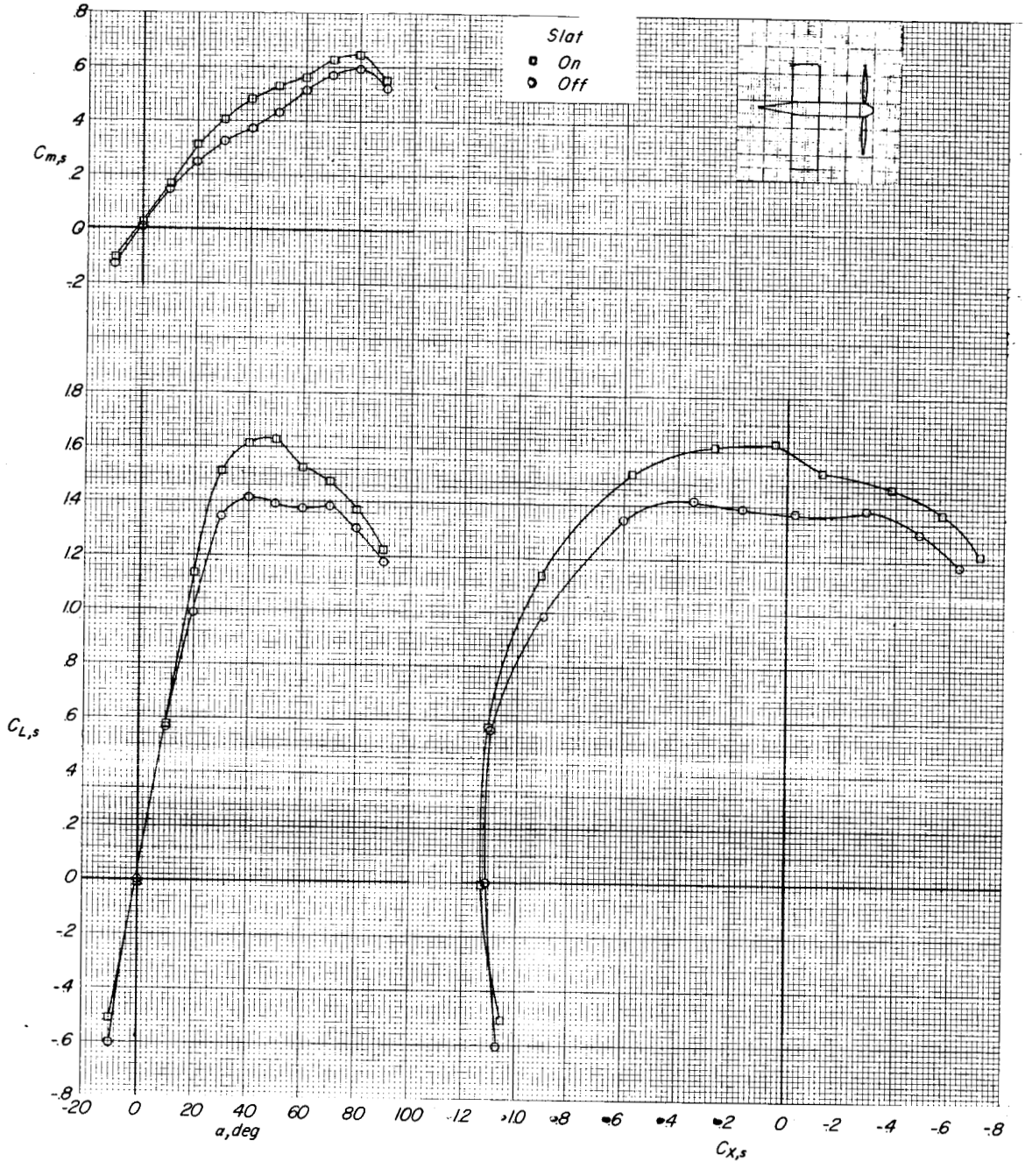

(c) $C_{T,s} = 0.58$.

Figure 7.- Continued.

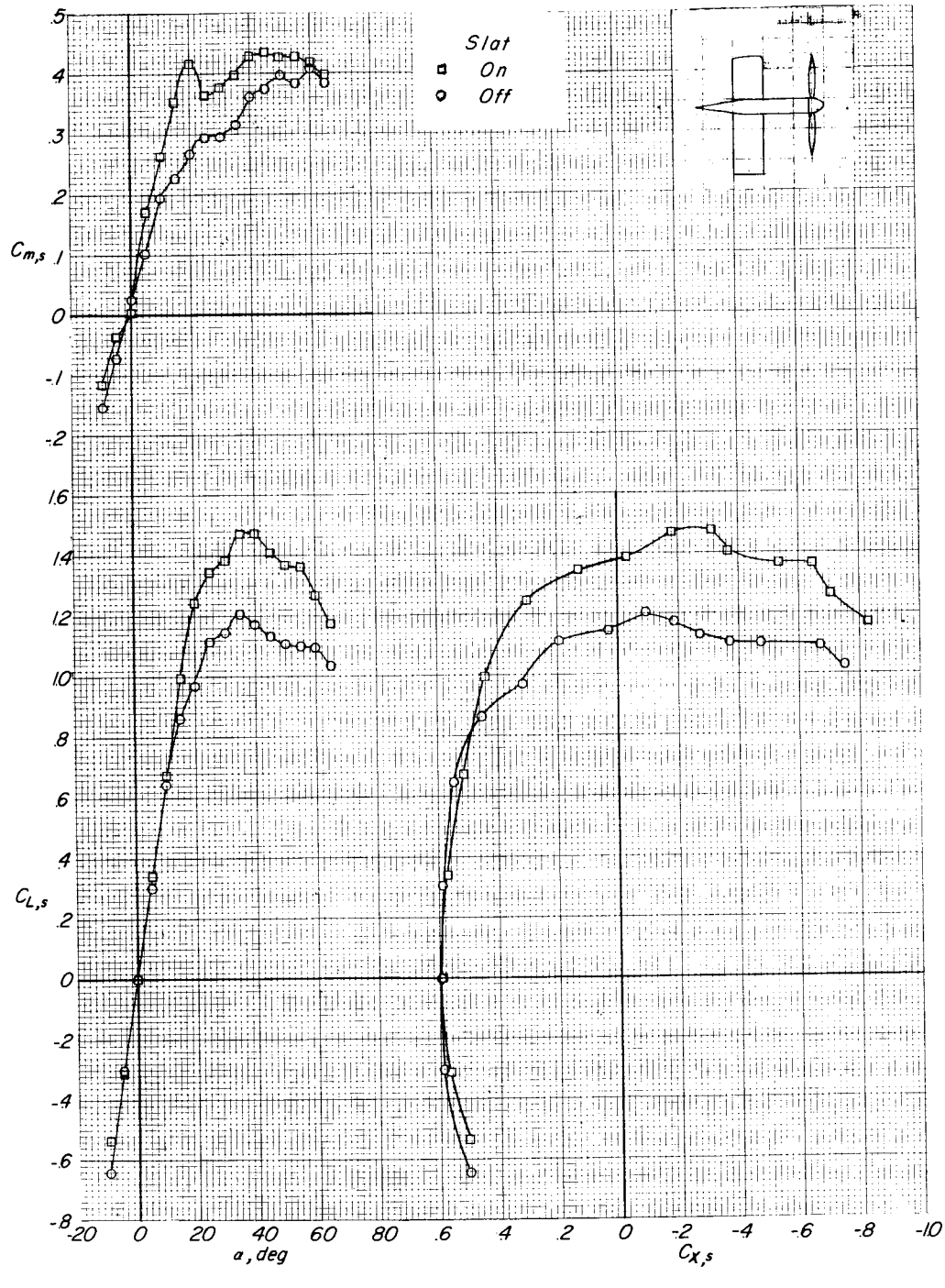

(d) $C_{T,s} = 0.27$.

Figure 7.- Continued.

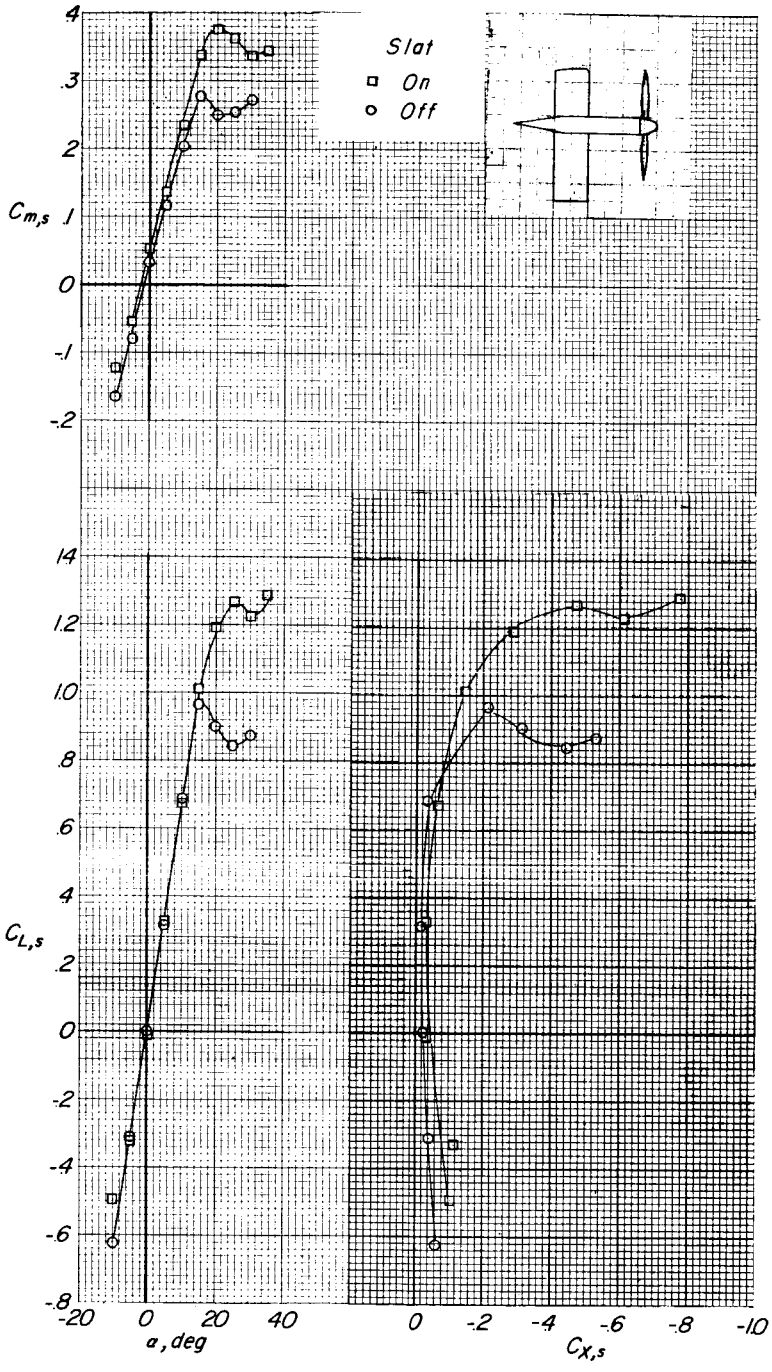

(e) $C_{T,s} = 0$.

Figure 7.- Concluded.

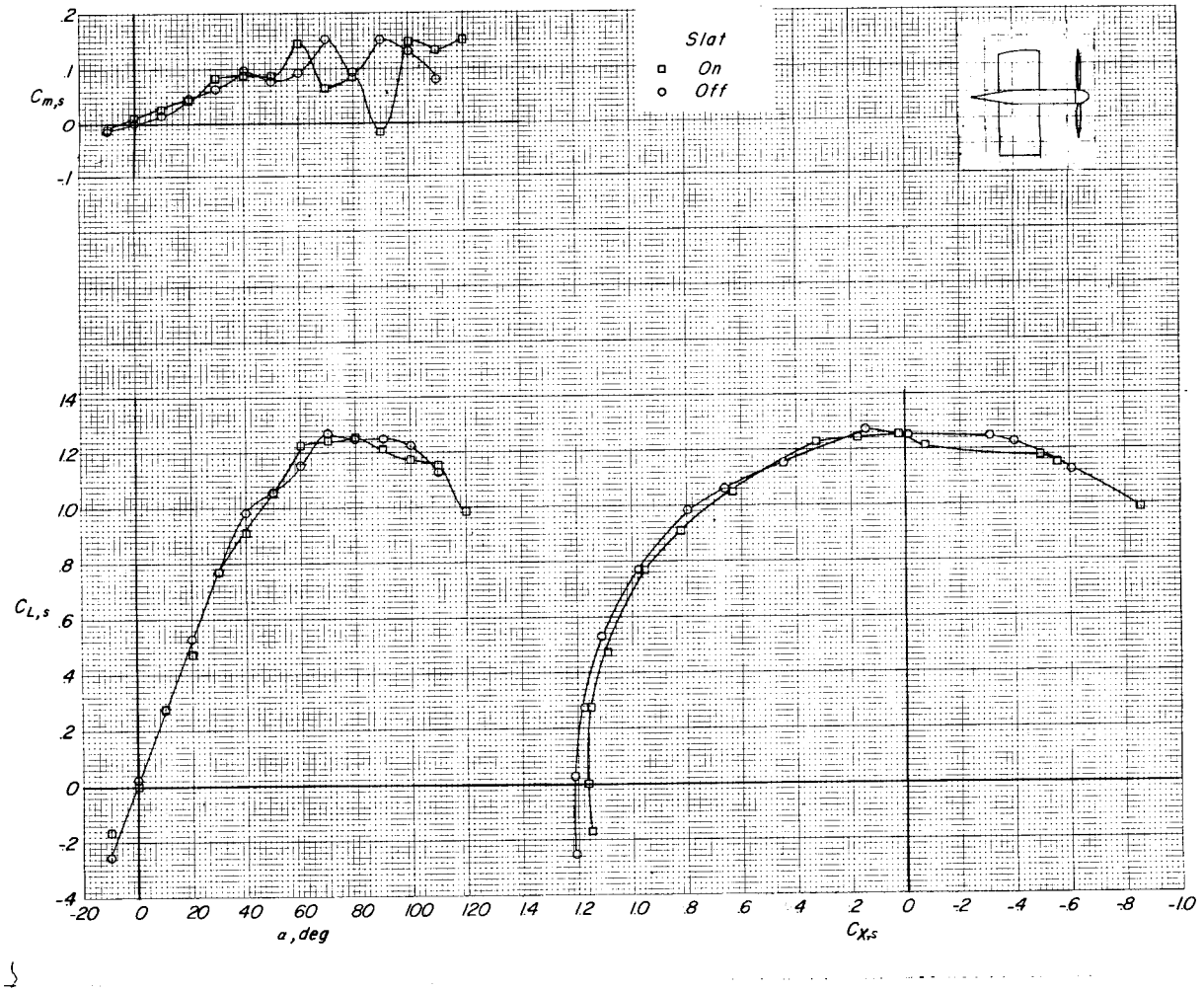

(a) $C_{T,s} = 0.98$.

Figure 8.- Longitudinal aerodynamic characteristics of model B (c/D = 0.50).

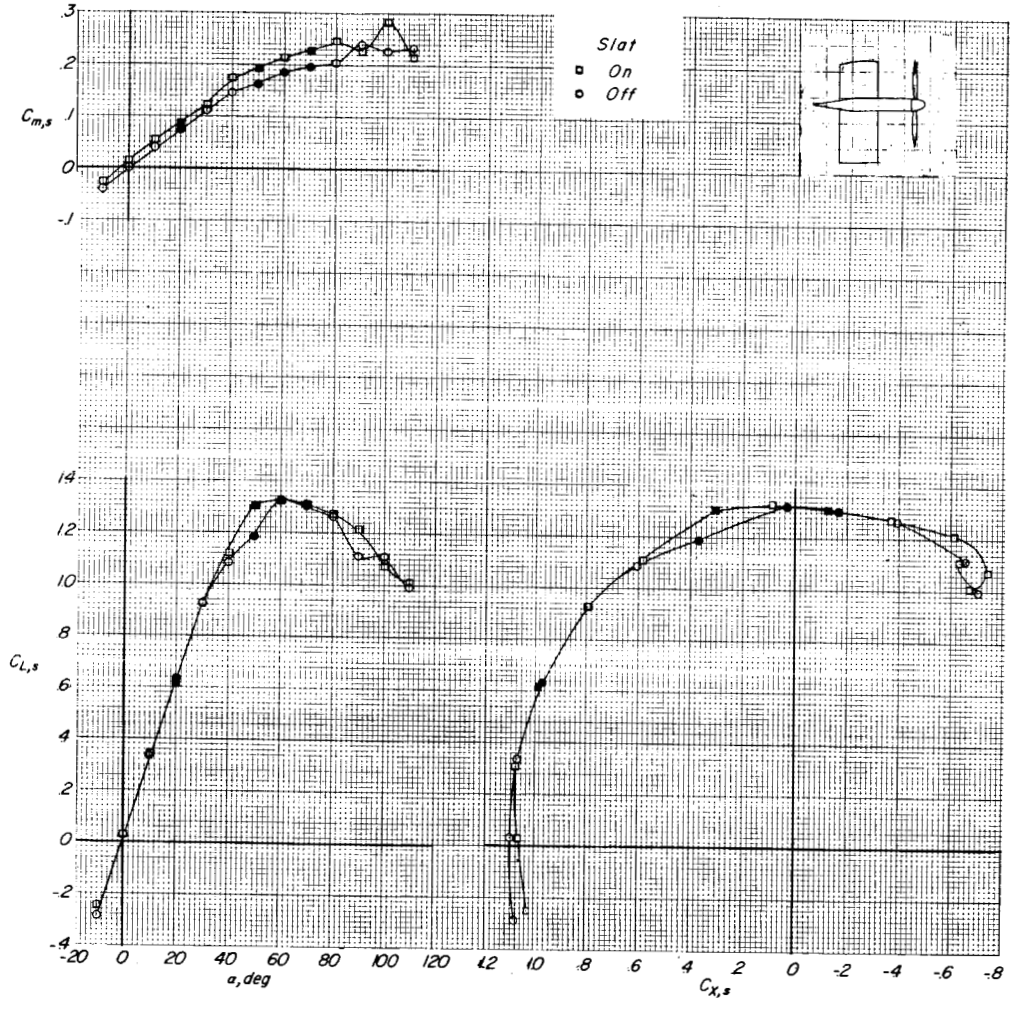

(b) $C_{T,s} = 0.88$.

Figure 8.- Continued.

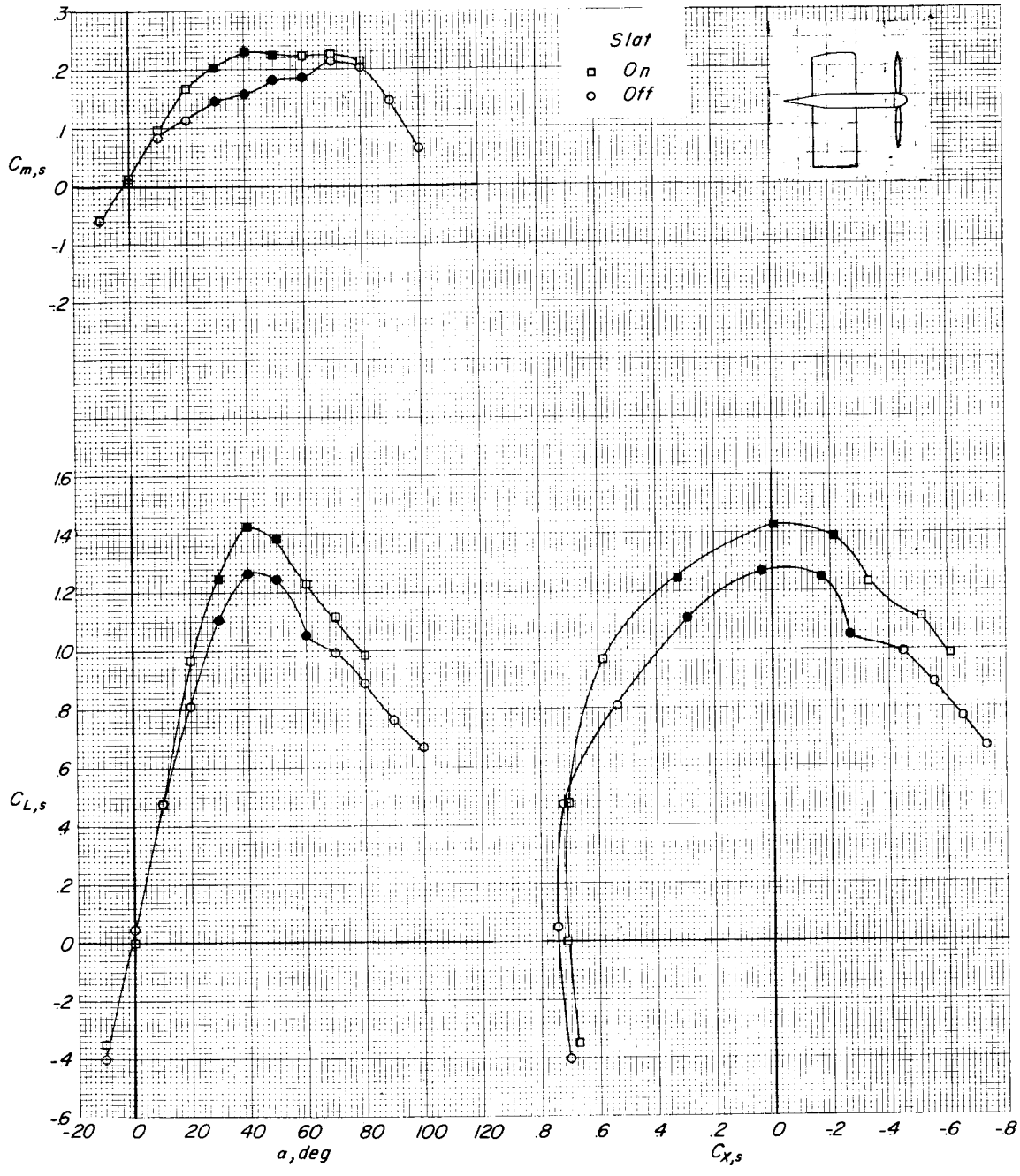

(c) $C_{T,s} = 0.58$.

Figure 8.- Continued.

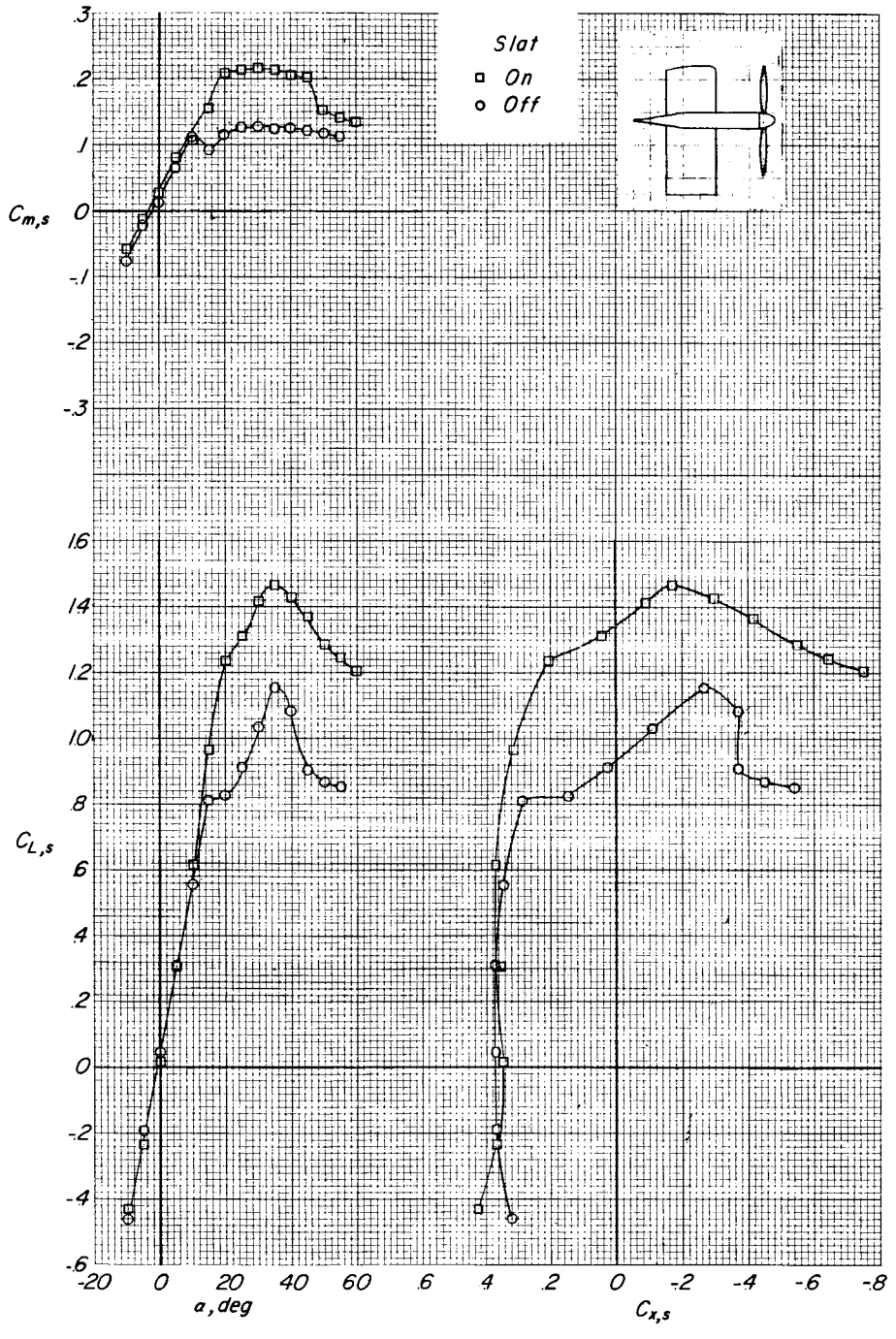

(d) $C_{T,s} = 0.27$.

Figure 8.- Continued.

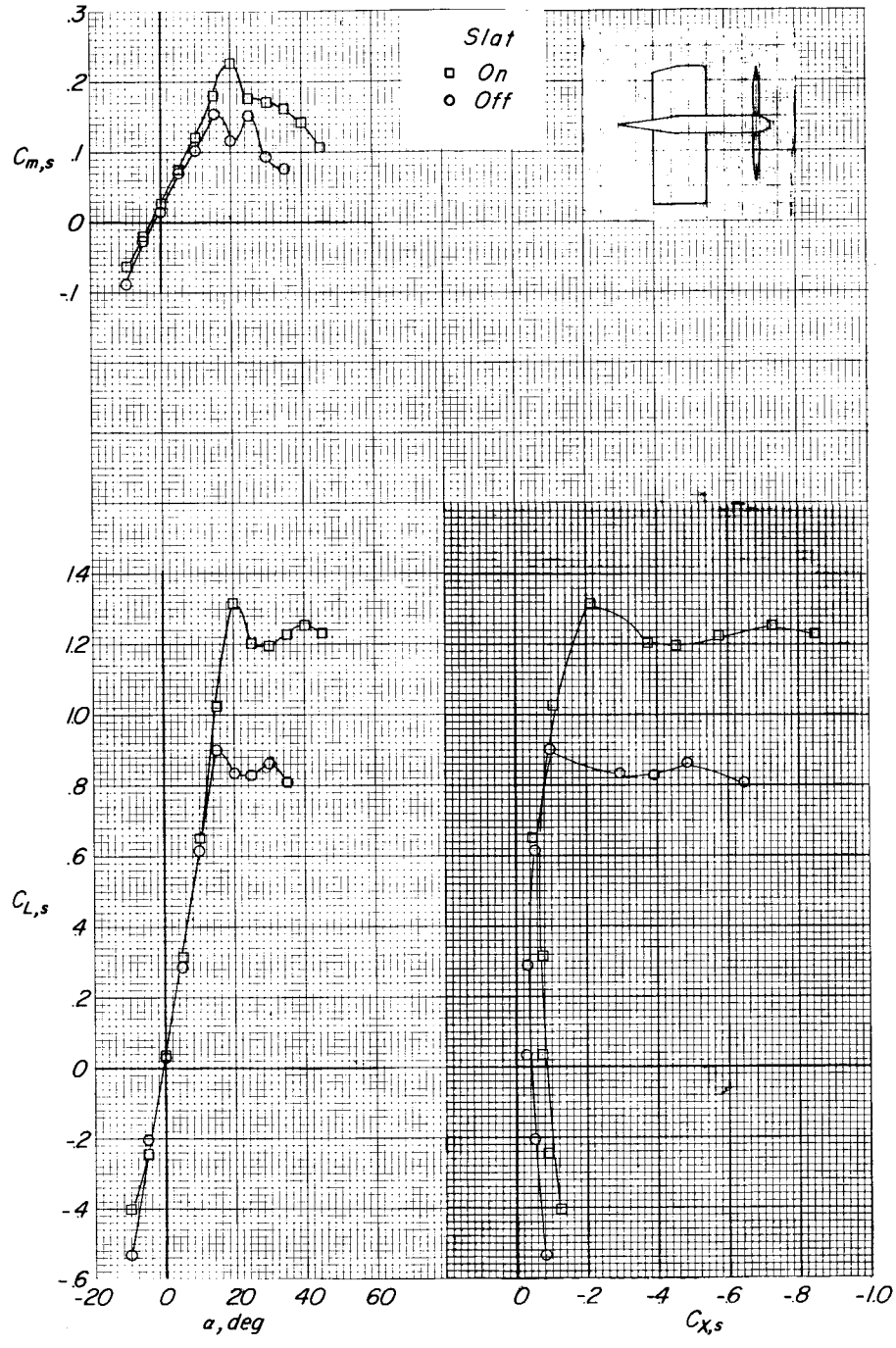

(e) $C_{T,s} = 0$.

Figure 8.- Concluded.

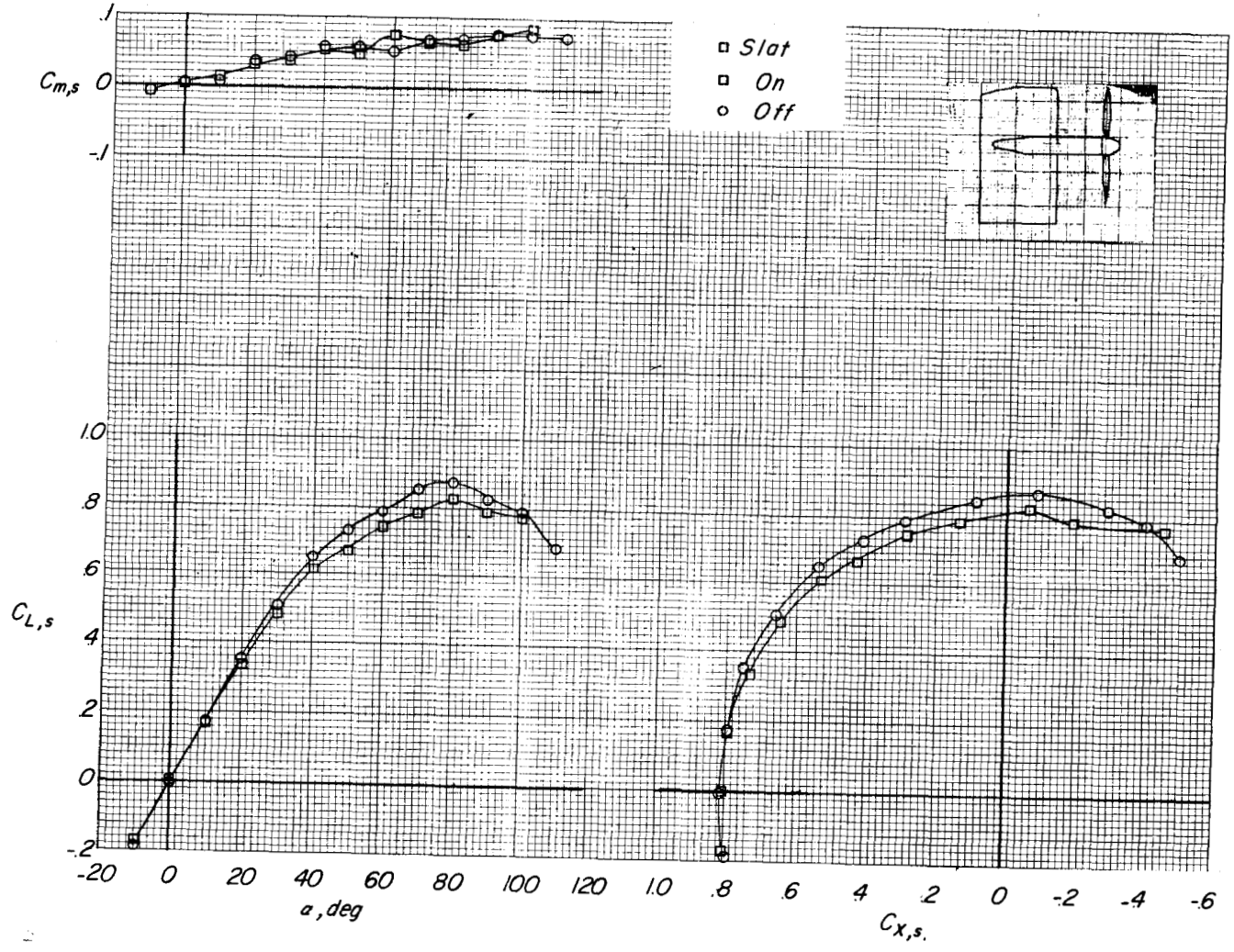

(a) $C_{T,s} = 0.98$.

Figure 9.- Longitudinal aerodynamic characteristics of model C (c/D = 0.75).

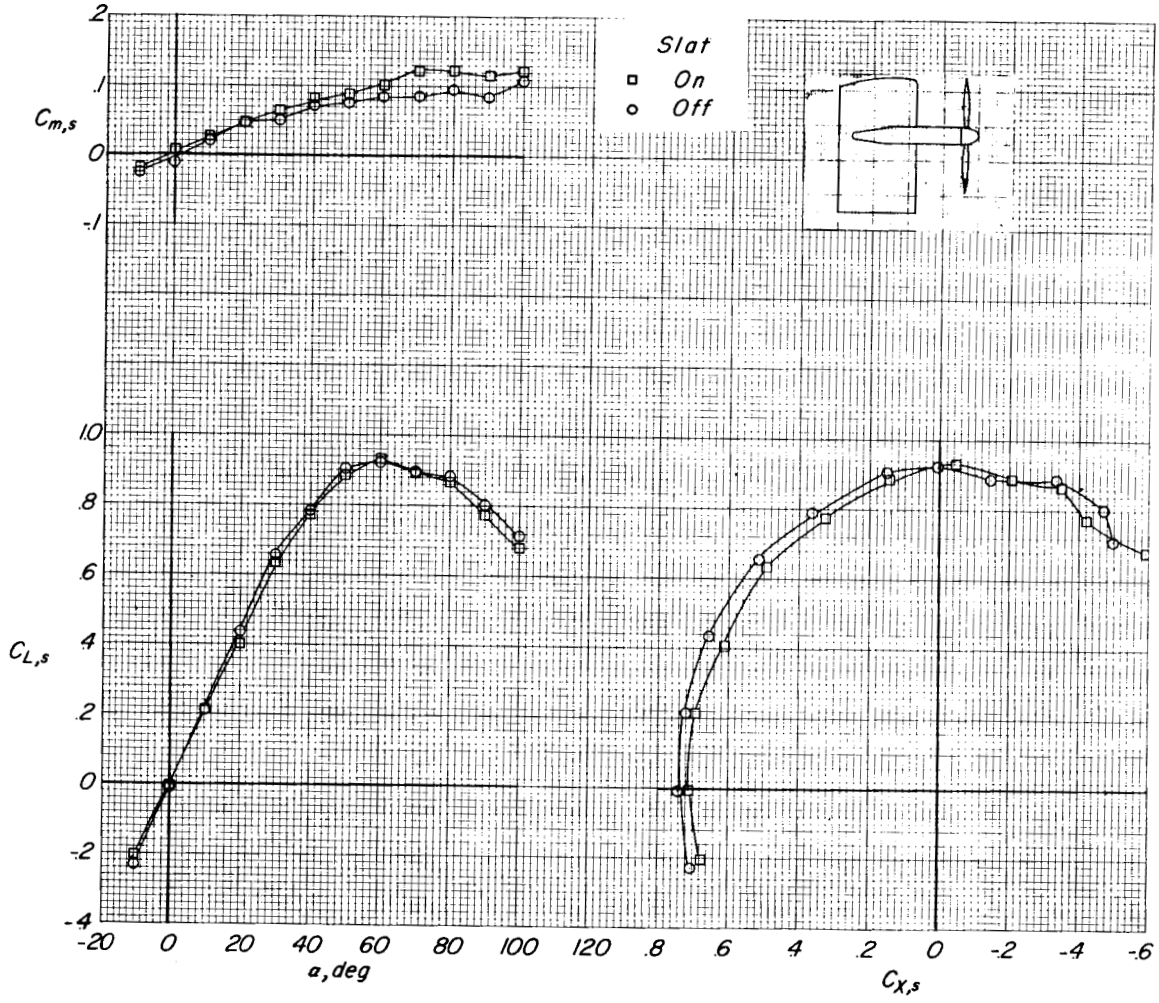

(b) $C_{T,s} = 0.89$.

Figure 9.- Continued.

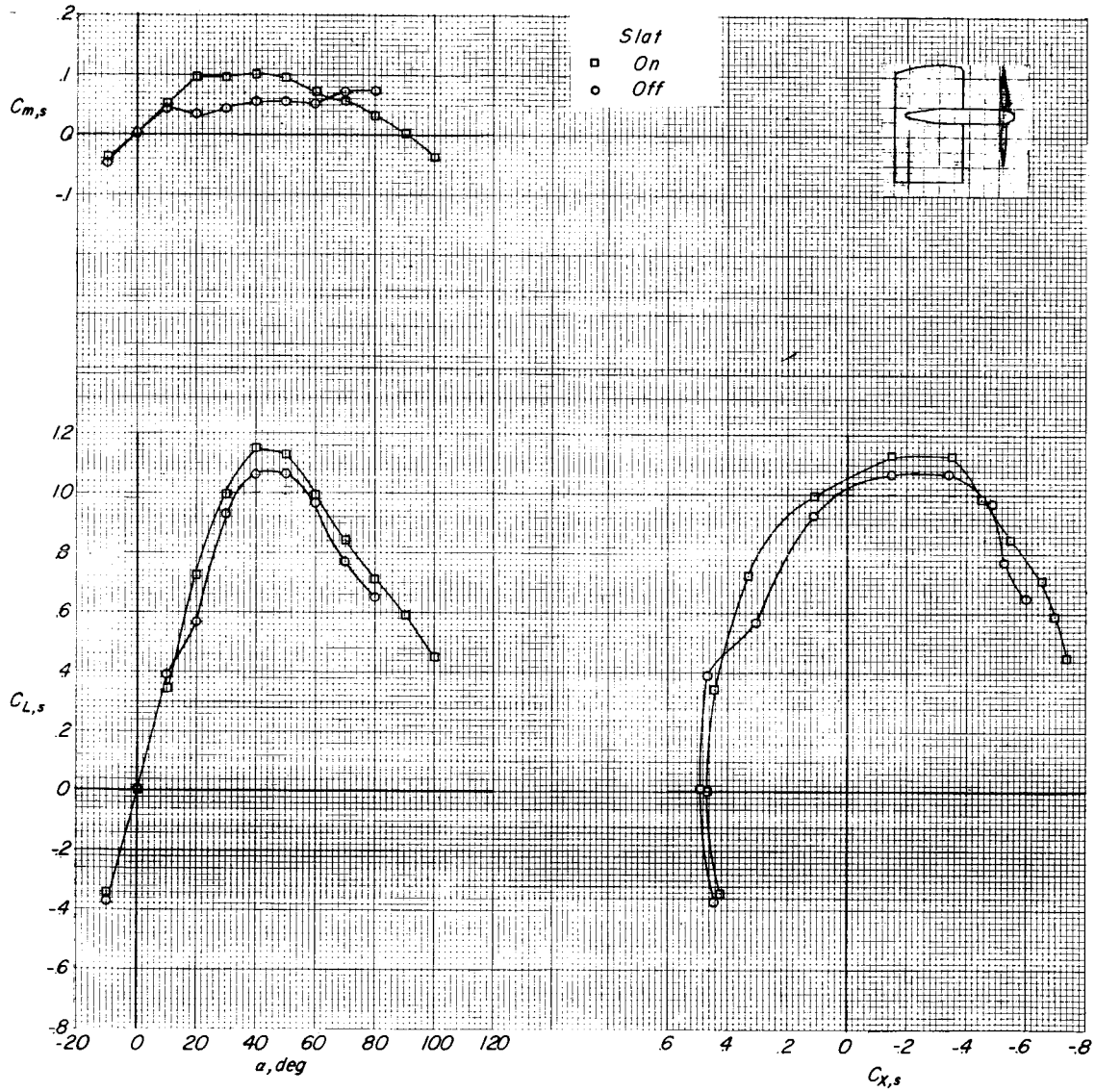

(c) $C_{T,s} = 0.57$.

Figure 9.- Continued.

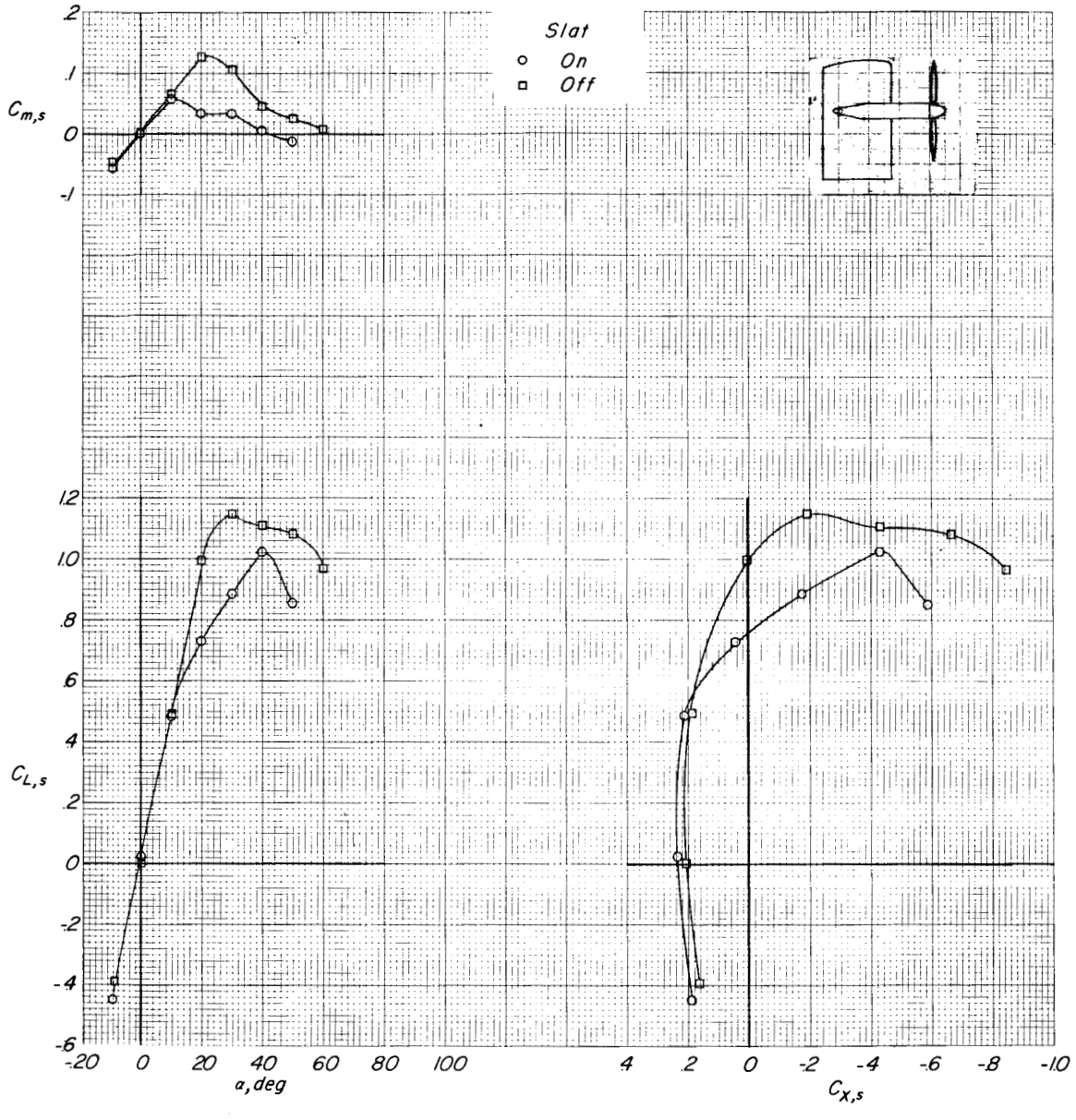

(d) $C_{T,s} = 0.27$.

Figure 9.- Continued.

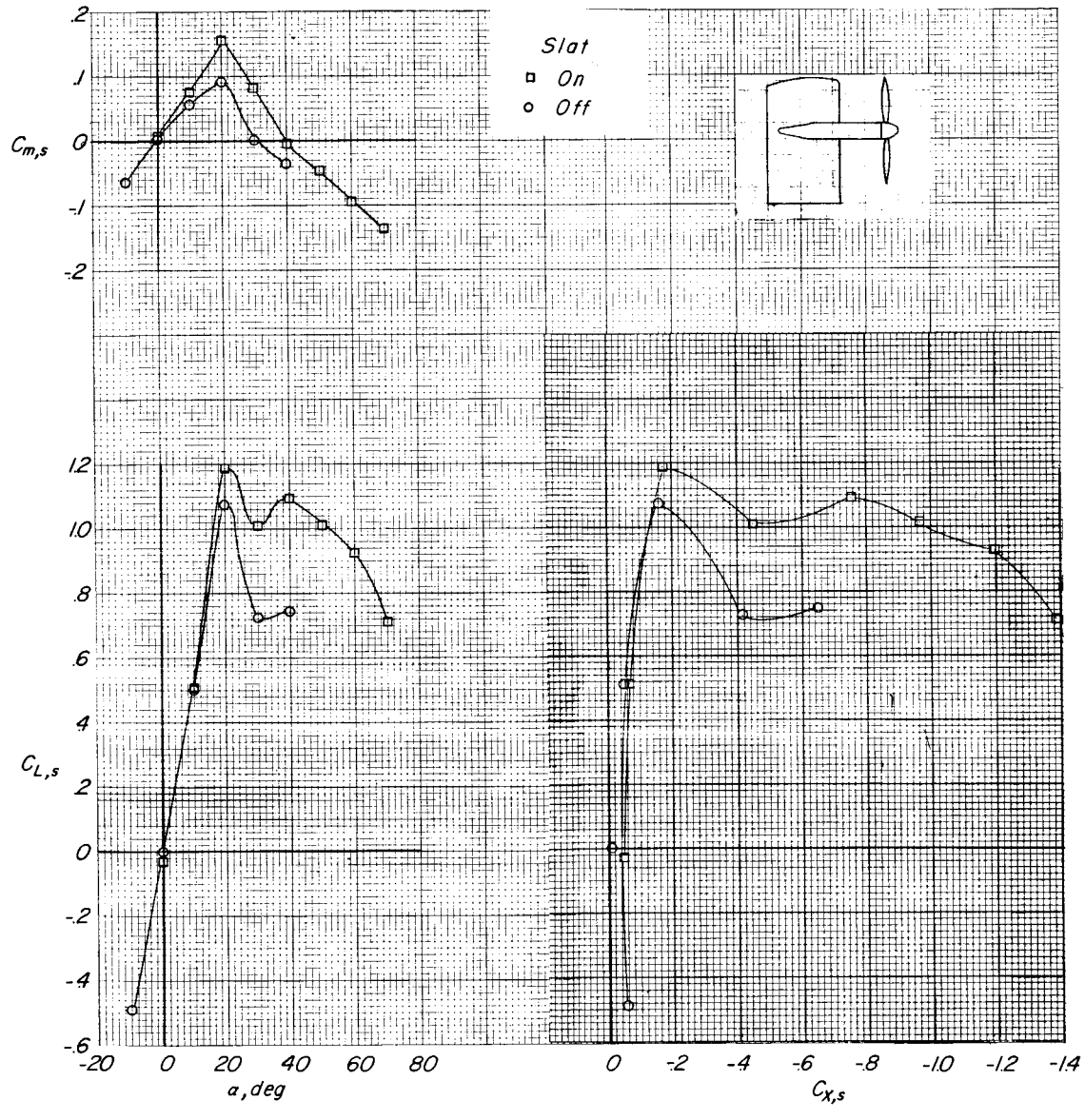

(e) $C_{T,s} = 0$.

Figure 9.- Concluded.

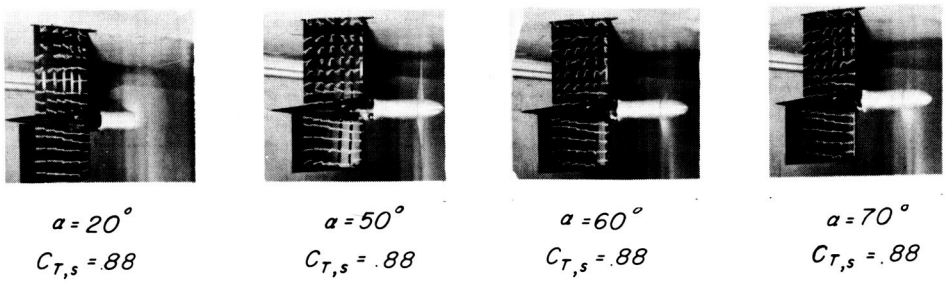

$\alpha = 20°$ $C_{T,s} = .88$ | $\alpha = 50°$ $C_{T,s} = .88$ | $\alpha = 60°$ $C_{T,s} = .88$ | $\alpha = 70°$ $C_{T,s} = .88$

Slat retracted

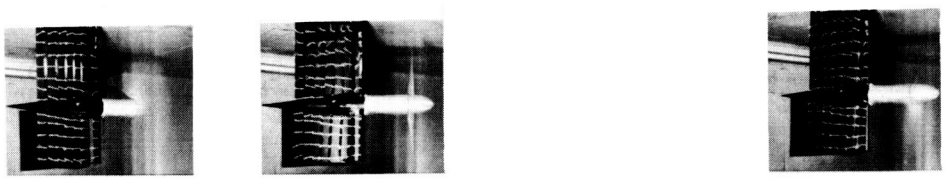

$\alpha = 20°$ $C_{T,s} = .88$ | $\alpha = 50°$ $C_{T,s} = .88$ | $\alpha = 70°$ $C_{T,s} = .88$

Slat extended

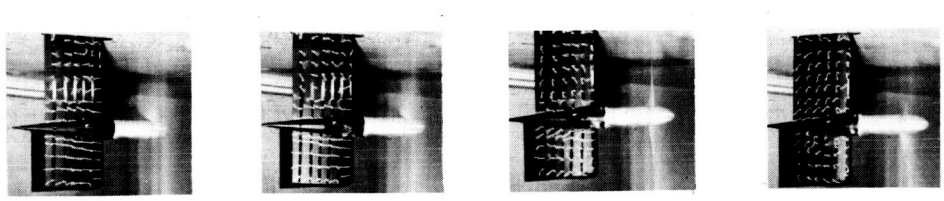

$\alpha = 30°$ $C_{T,s} = .58$ | $\alpha = 40°$ $C_{T,s} = .58$ | $\alpha = 50°$ $C_{T,s} = .58$ | $\alpha = 60°$ $C_{T,s} = .58$

Slat retracted

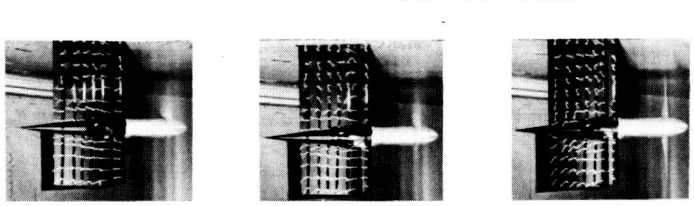

$\alpha = 30°$ $C_{T,s} = .58$ | $\alpha = 40°$ $C_{T,s} = .58$ | $\alpha = 50°$ $C_{T,s} = .58$

Slat extended

L-59-1933

Figure 10.- Photographs of the stall pattern as indicated by wool tufts on the upper surface of the wing. Model B.

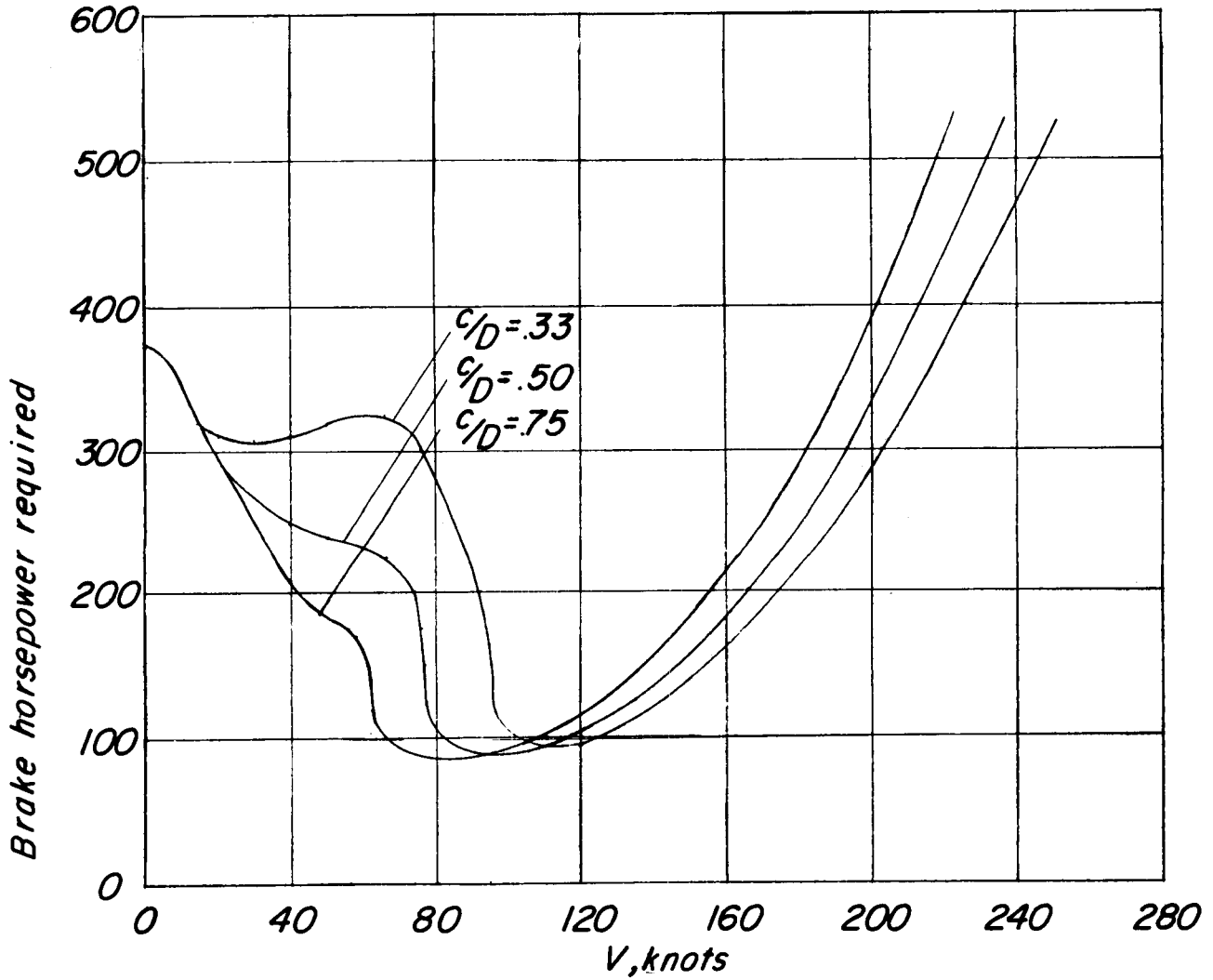

Figure 11.- Effect of changes in c/D on horsepower required for an assumed airplane in steady level flight with slat retracted.

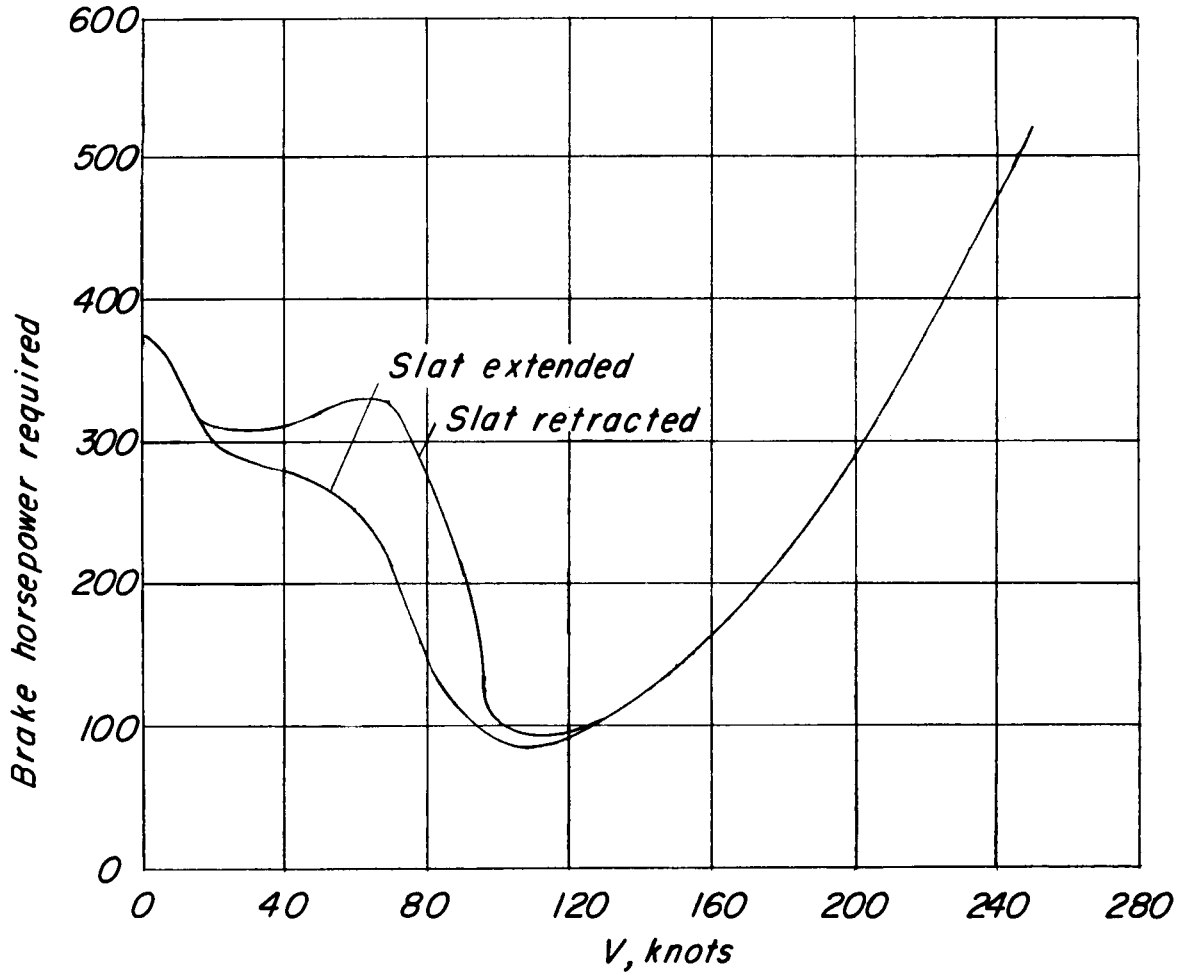

(a) c/D = 0.33.

Figure 12.- Effect of addition of a stall-control slat on horsepower required for an assumed airplane in steady level flight.

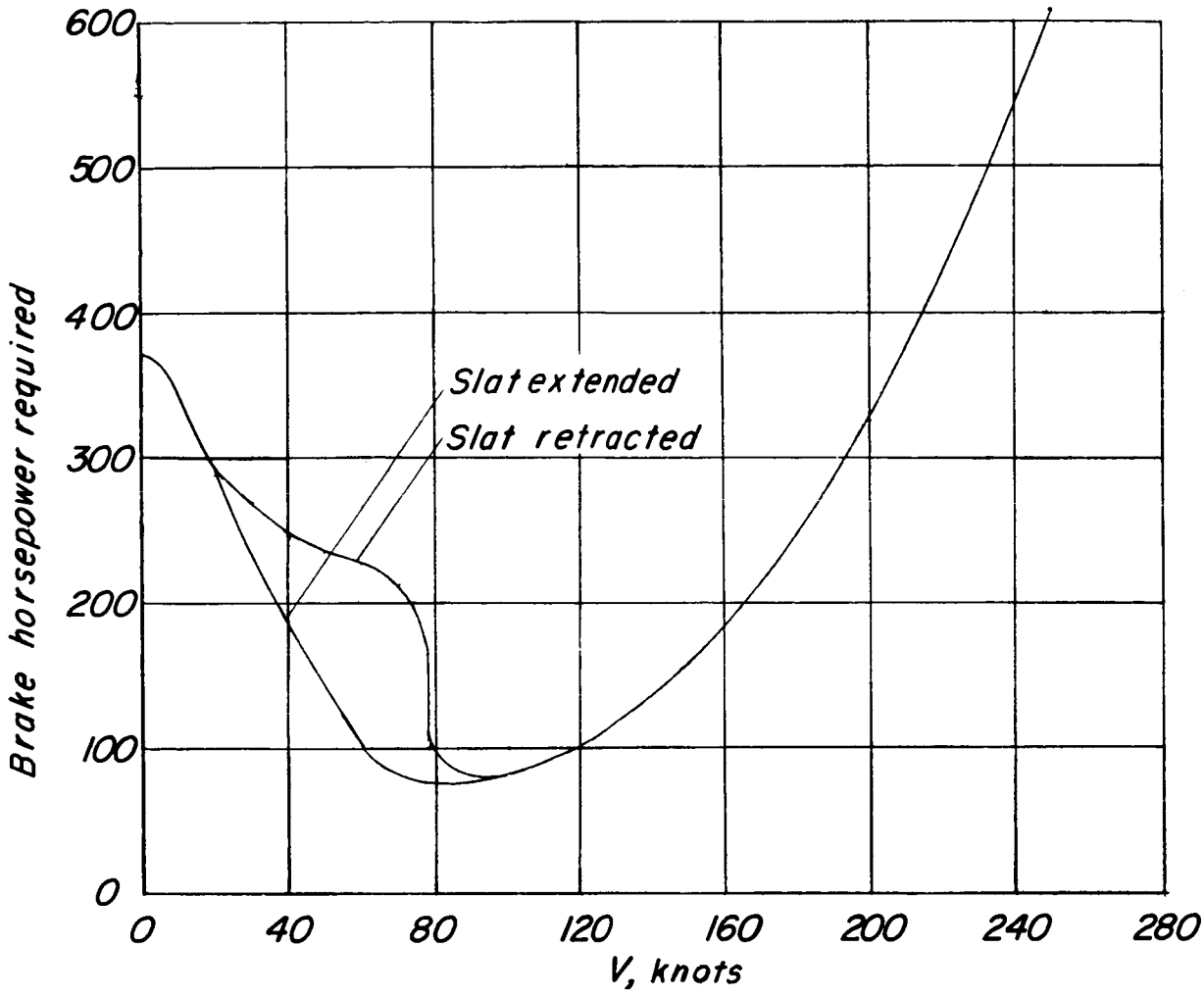

(b) c/D = 0.50.

Figure 12.- Continued.

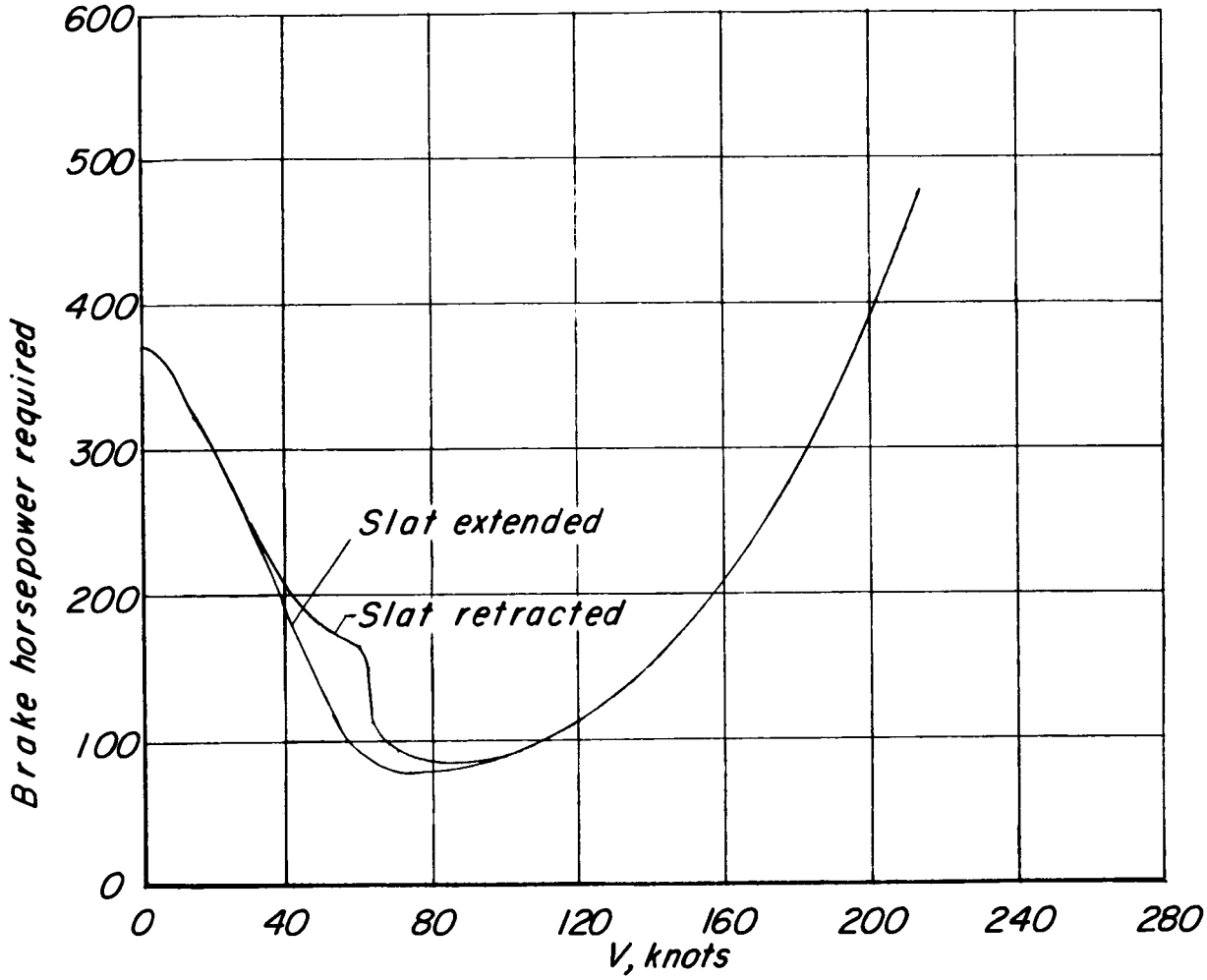

(c) c/D = 0.75.

Figure 12.- Concluded.

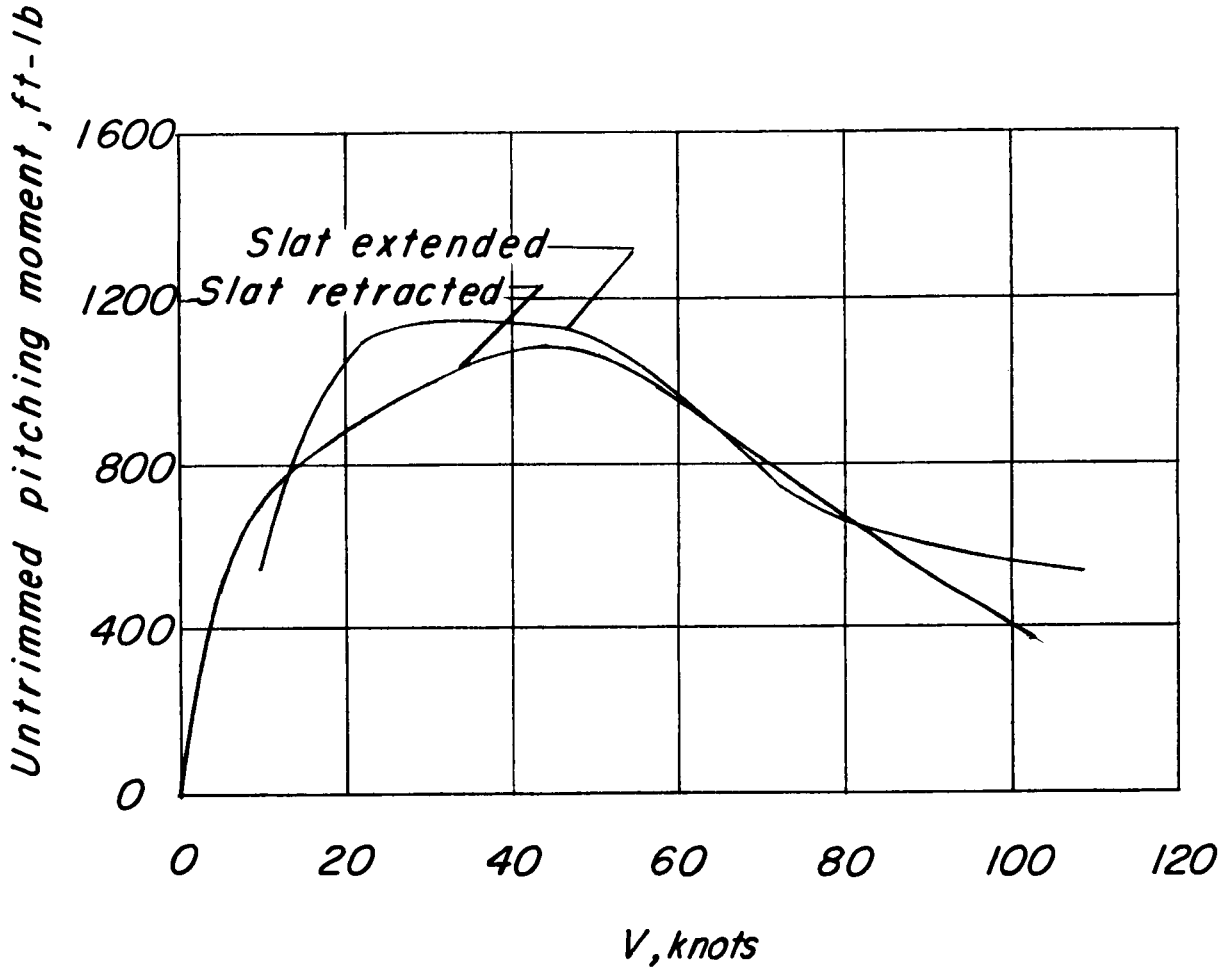

(a) c/D = 0.33.

Figure 13.- Effect of addition of a stall-control slat on the untrimmed pitching moment of an assumed airplane in steady level flight.

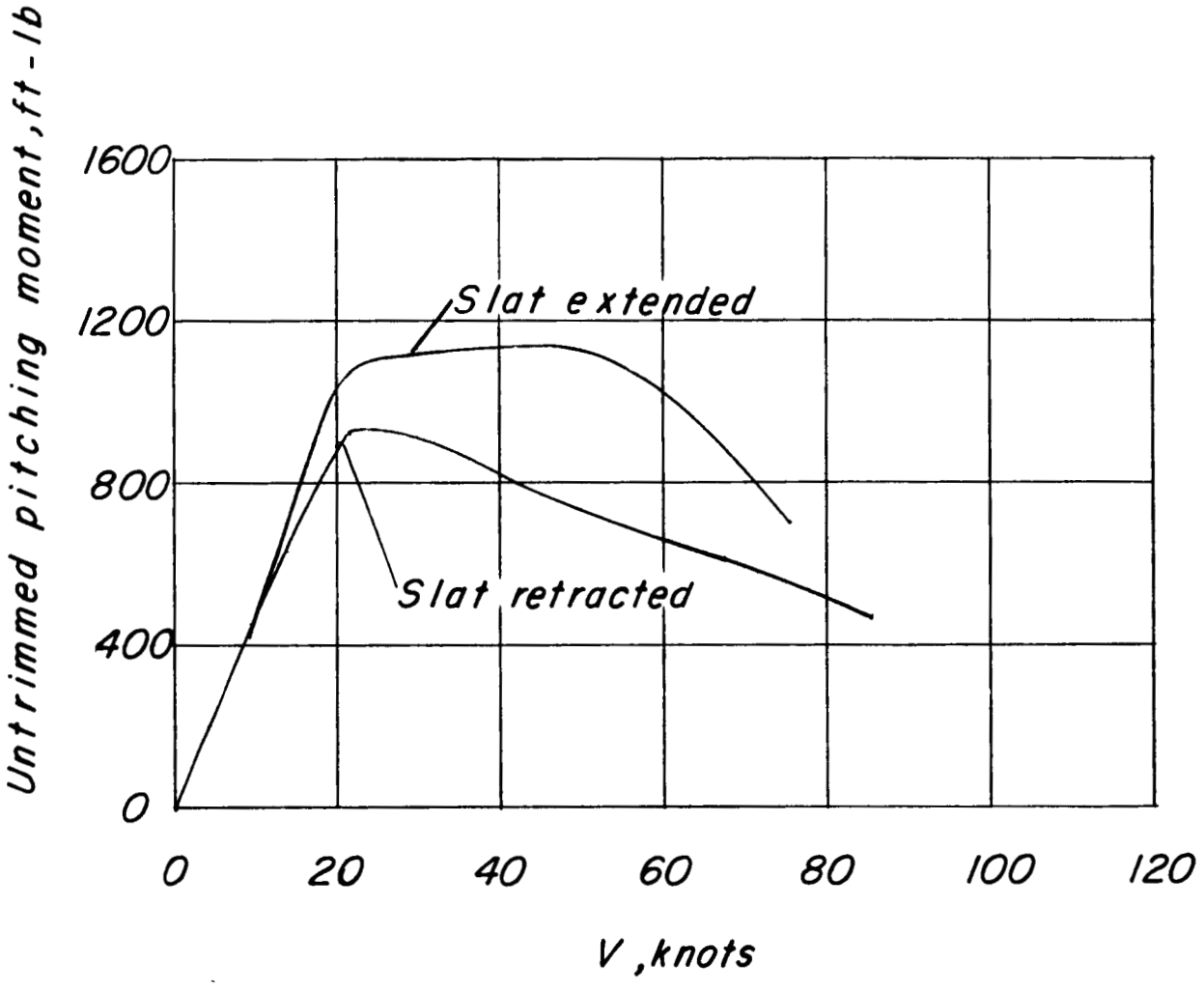

(b) c/D = 0.50.

Figure 13.- Continued.

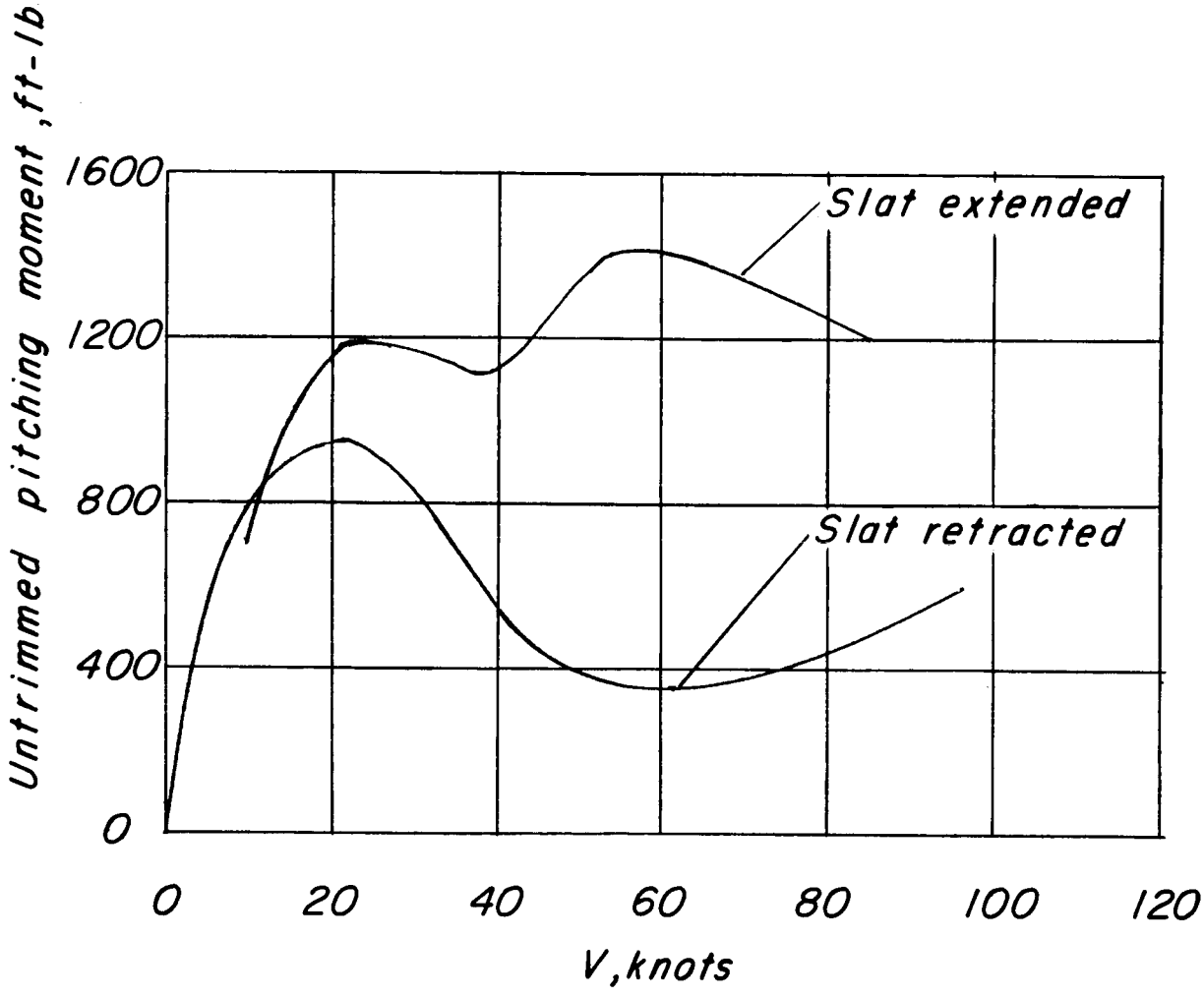

(c) c/D = 0.75.

Figure 13.- Concluded.

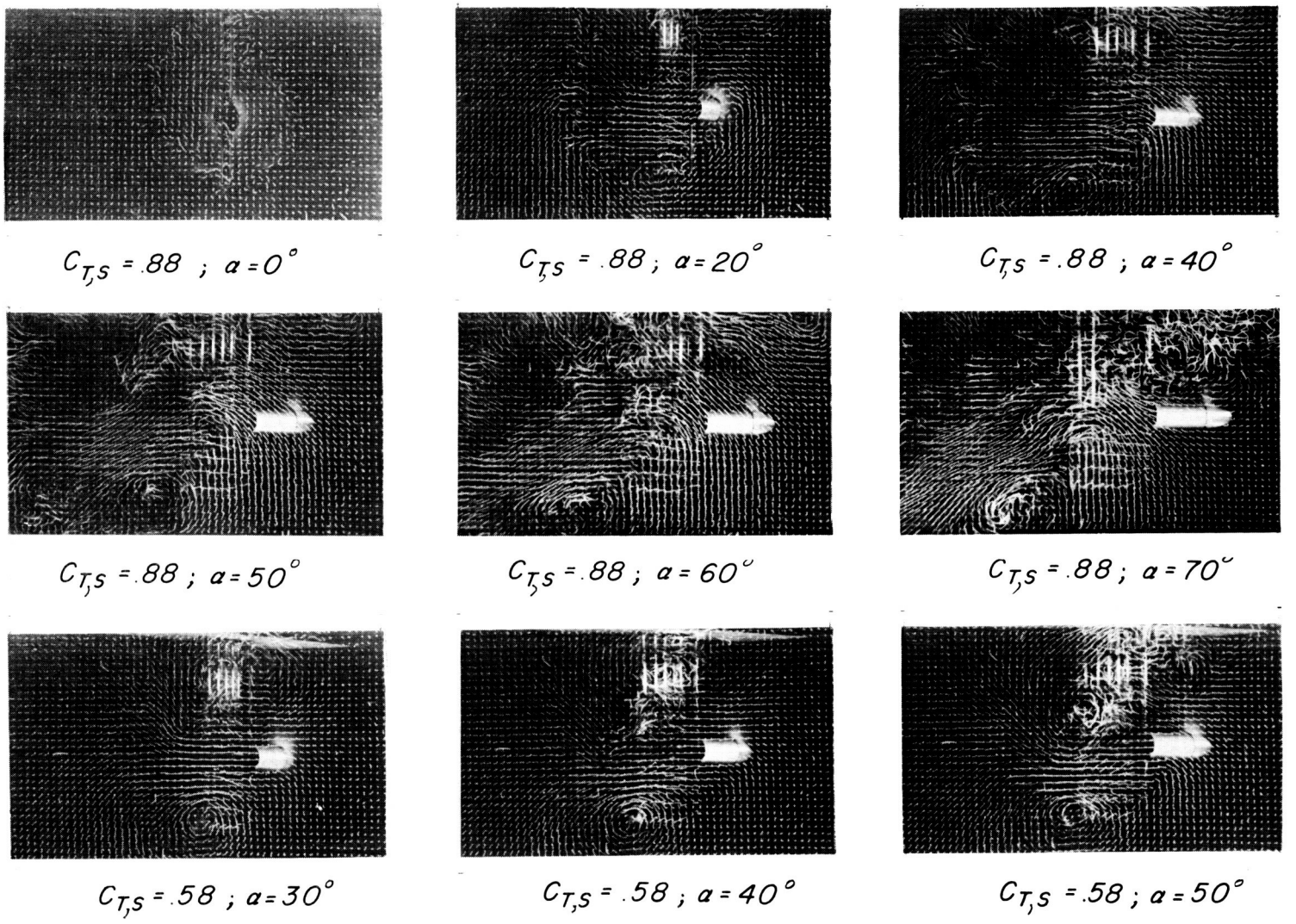

L-59-1932

Figure 14.- Photographs of flow pattern at an assumed tail location as indicated by a tuft grid. Model B (c/D = 0.50); slat extended.